Susanne Maria Bauer, BSc

Modeling and Simulation of Conducted Disturbances in Automotive Systems

MASTERARBEIT

zur Erlangung des akademischen Grades

Diplom-Ingenieur

Masterstudium Telematik

eingereicht an der

Technischen Universität Graz

Betreuer: Ass.Prof. Dipl.-Ing. Dr.techn. Gunter Winkler

Institut für Elektronik

Head: Univ.-Prof. Dipl-Ing. Dr.techn. Bernd Deutschmann

Graz, Mai 2014

This document is set in Palatino, compiled with pdfLaTeX2e and `Biber`.

The LaTeX template from Karl Voit is based on KOMA script and can be found online: https://github.com/novoid/LaTeX-KOMA-template

EIDESSTATTLICHE ERKLÄRUNG

AFFIDAVIT

Ich erkläre an Eides statt, dass ich die vorliegende Arbeit selbstständig verfasst, andere als die angegebenen Quellen/Hilfsmittel nicht benutzt, und die den benutzten Quellen wörtlich und inhaltlich entnommenen Stellen als solche kenntlich gemacht habe. Das in TUGRAZonline hochgeladene Textdokument ist mit der vorliegenden Masterarbeit identisch.

I declare that I have authored this thesis independently, that I have not used other than the declared sources/resources, and that I have explicitly indicated all material which has been quoted either literally or by content from the sources used. The text document uploaded to TUGRAZonline is identical to the present master's thesis.

Graz, _____ _____

Datum/Date Unterschrift/Signature

Abstract

The development of electric and hybrid vehicles poses new challenges for meeting the EMC requirements. Simulations therefore are getting more and more important as an early evaluation method.
In this work the main focus is to model the high voltage cables and simulate the conducted disturbances.
One part provides a simulation model for the Capacitive Coupling Clamp regarding *ISO 7637-3:2007*, respectively regarding *IEC 61000-4-4* for transient immunity testing.
The second part focuses on simulating interferences, that are generated by the DC/AC Power converter and the inferences generated by the overall electric drive system.

Contents

1 Overview

The trend regarding automotive vehicles tends more and more towards electric drives. In hybrid cars the integration of the high voltage electric power train, illustrated in figure (1.1)), is an essential requirement.

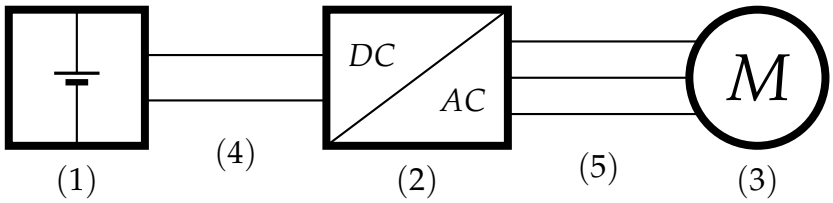

Figure 1.1: Power Train of Hybrid Car

The main components are:

1. Traction Battery (Lithium Ion- Battery)
2. Power Converter (realized with *IGBTs*)
3. Motor
4. HV-cable, shielded, single wire
5. HV-motor cable, shielded, three wire

The standard specifications regarding electromagnetic compatibility (EMC) are high and very challenging to meet. In this work the main focus is to derive simulation models to predict conducted disturbances on high voltage cables.

Chapter (2) provides a short overview of the test pulses used for transient testing and their causations.(**1**)

Chapters (3) and (4) give a short overview of the cable theory, that is needed for the modeling and illustrate the implementation of a simulation model cable.

In chapters (5) and (6) a model for the Capacitive Coupling Clamp for fast transient testing is provided, as stated in (**1**) and (**2**).

In Chapter (7) the main focus is on simulating the conducted disturbances on the high voltage path between the power converter and the battery, as depicted in the simplified diagram in figure (1.1). There is also an attempt to simulate the disturbances generated by the overall electric drive system.

2 Test Pulses

The test pulses are defined in the international standard ISO 7637-2, third edition (**1**).

Supply Voltage	$12V$ System in $[V]$	$24V$ System in $[V]$
U_A	13.5 ± 0.5	27 ± 1

2.1 Test Pulse 1

This test pulse represents impulses, that are caused by switching of inductive loads.
It is used in cases, where the device under test (DUT) is connected in the automotive electrical system in such a way, that after switching off the inductive load the DUT is still parallel to the load.
The supply voltage of the DUT is switched off while it is supplied with the test pulse. The principle for this test pulse is demonstrated in figure (2.1). Its shape and parameters are shown in figure (2.2) and in table (2.1).

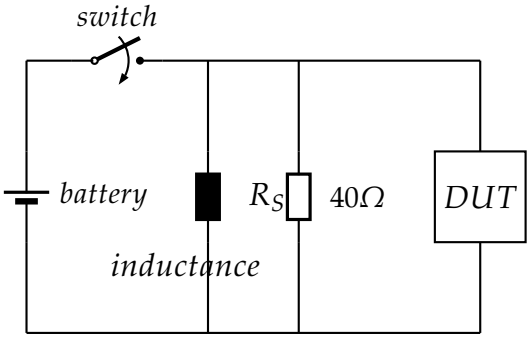

Figure 2.1: Principle for Test Pulse 1

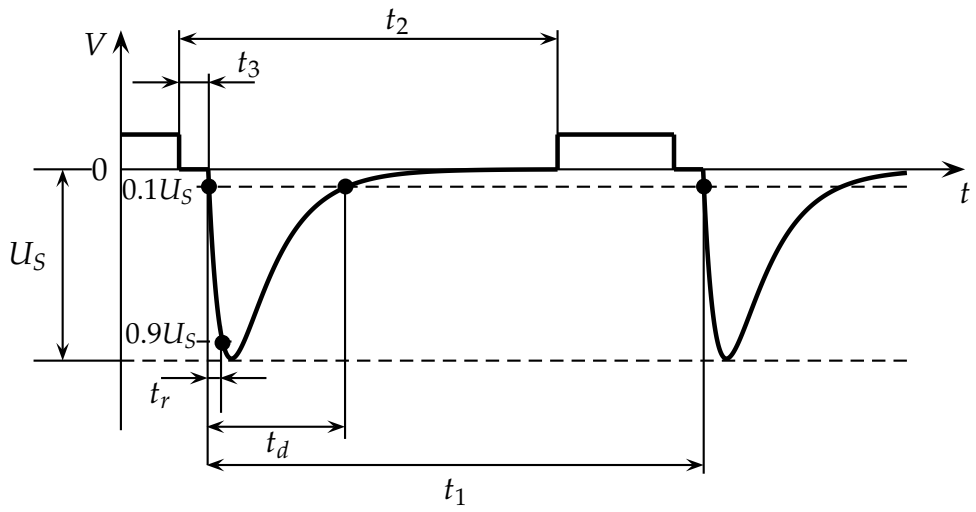

Figure 2.2: Test Pulse 1

Parameters	Nominal 12 V system	Nominal 24V system
U_S	$-75V \ldots -150V$	$-300 \ldots -600V$
R_i	10Ω	50Ω
t_d	$2ms$	$1ms$
t_r	$\left(1\ {}^{0}_{-0.5}\right)\ \mu s$	$\left(3\ {}^{0}_{-1.5}\right)\ \mu s$
t_1	$\geq 0.5s$	
t_2	$200ms$	
t_3	$< 100\mu s$	

Table 2.1: Parameters for Test Pulse 1

2.2 Test Pulses 2a and 2b

Test Pulse 2a

Test Pulse 2a models transient pulses that are caused due to sudden interruption of currents of a device, that is connected in the automotive electrical system in parallel with the DUT.
The pulse intensity depends on the inductance of the wiring harness. The battery voltage is not switched off, therefore this test is a functional test.
The principle for this test pulse is demonstrated in figure (2.3). Its shape and parameters are shown in figure (2.4) and in table (2.2)

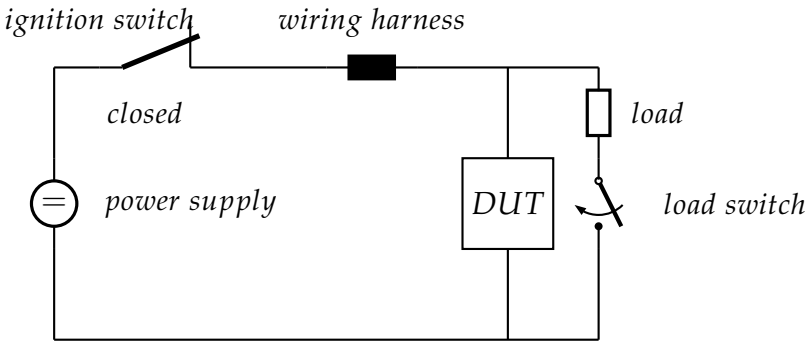

Figure 2.3: Principle for Test Pulse 2a

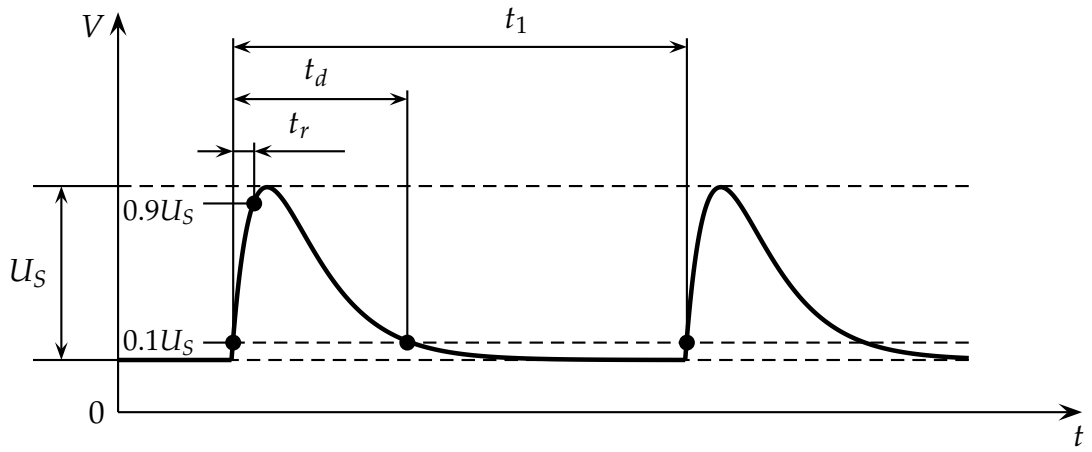

Figure 2.4: Test Pulse 2a

Parameters	Nominal $12V$ and $24V$ system
U_S	$+37V \ldots + 112V$
R_i	2Ω
t_d	$0.05ms$
t_r	$(1\ {}^{0}_{-0.5})\ \mu s$
t_1	$0.2s \ldots 5s$

Table 2.2: Parameters for Test Pulse 2a

Test Pulse 2b

This pulse models transient pulses, which are caused by DC-motors, which are connected in parallel with the DUT via the automotive electrical system. After the supply voltage of the motor is switched off, the motor acts as a generator.

The principles is demonstrated in figure (2.5). The shape of the test pulse and its parameters are shown in figure (2.6) and in table (2.3).

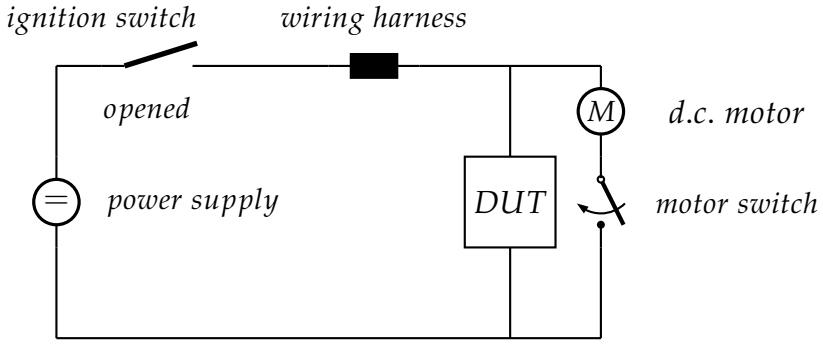

Figure 2.5: Principle for Test Pulse 2b

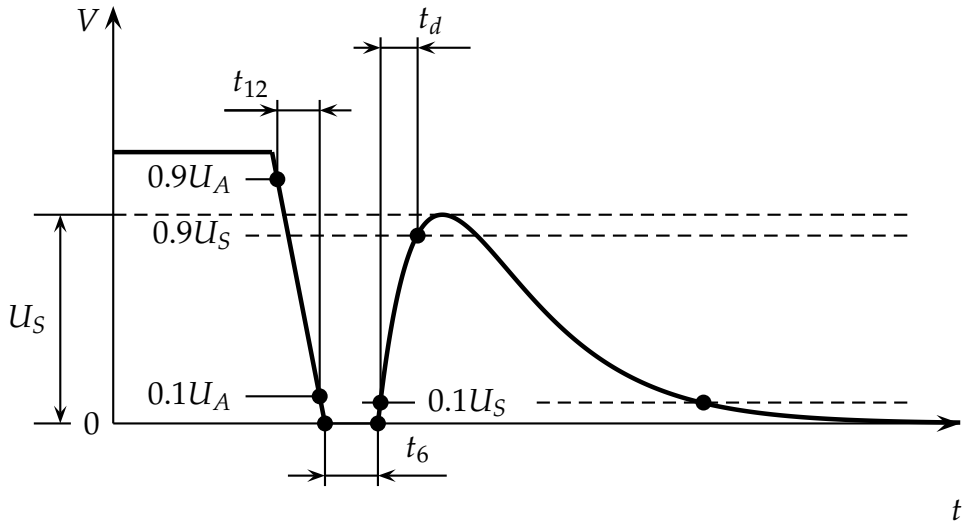

Figure 2.6: Test pulse 2b

Parameters	Nominal $12V$ system	Nominal $24V$ system
U_S	$10V$	$20V$
R_i	$0\Omega \ldots 0.05\Omega$	
t_d	$0.2s \ldots 2s$	
t_{12}	$1ms \pm 0.5ms$	
t_r	$1ms \pm 0.5ms$	
t_6	$1ms \pm 0.5ms$	

Table 2.3: Parameters for Test Pulse 2b

2.3 Test Pulses 3a and 3b

These test pulses model transients, that are results of switching processes. The characteristics of these transients are influenced by the wiring harness, since they consist of distributed inductances and capacitances.
When switching off inductive loads, voltage spikes with magnitudes of several thousand volts can occur.
The burst events last some milliseconds and every single pulse has a slope in the range of nanoseconds. Therefore they produce a very broadband interference spectrum.
The principle of this pulses is demonstrated in figure (2.7). The pulse shape and parameters for the Test Pulse 3a are shown in figure (2.8) and table (2.4).
For the Test pulse 3b it is depicted in figure (2.9) and table (2.5).

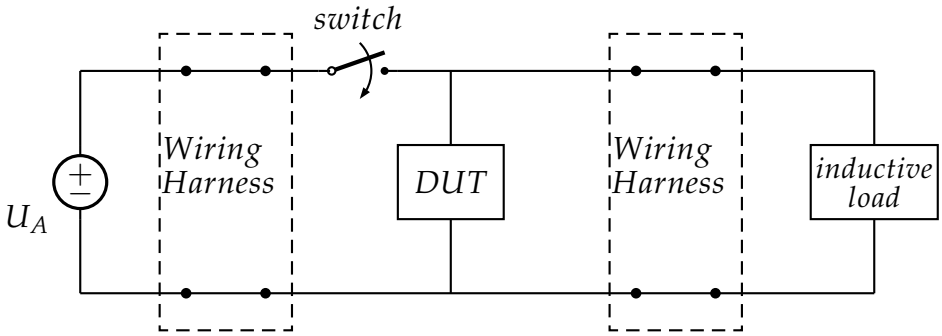

Figure 2.7: Principle for Test Pulses 3a and 3b

Test Pulse 3a

Burst

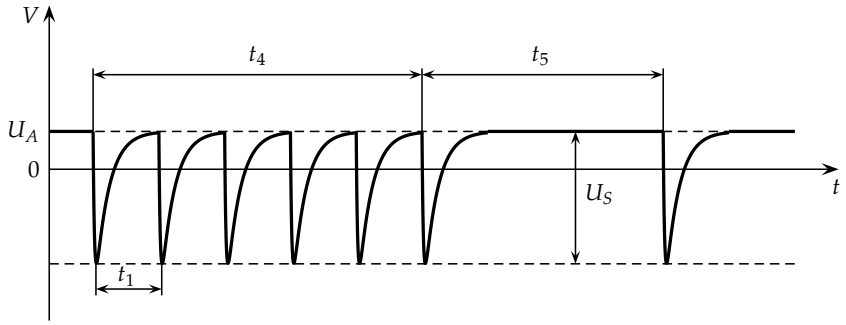

Single Pulse

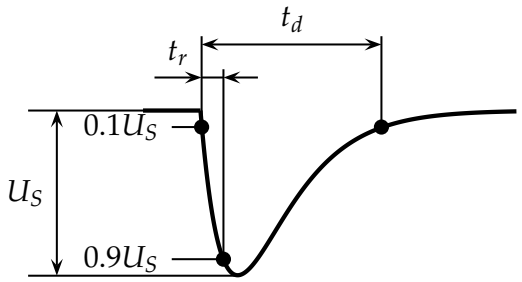

Figure 2.8: Test Pulse 3a

Parameters	Nominal $12V$ system	Nominal $24V$ system
U_S	$-112V \ldots -220V$	$-150 \ldots -300V$
R_i	50Ω	
t_d	$150ns \pm 45ns$	
t_r	$5ns \pm 1.5ns$	
t_1	$100\mu s$	
t_4	$10ms$	
t_5	$90ms$	

Table 2.4: Parameters for Test Pulse 3a

Test Pulse 3b

Burst

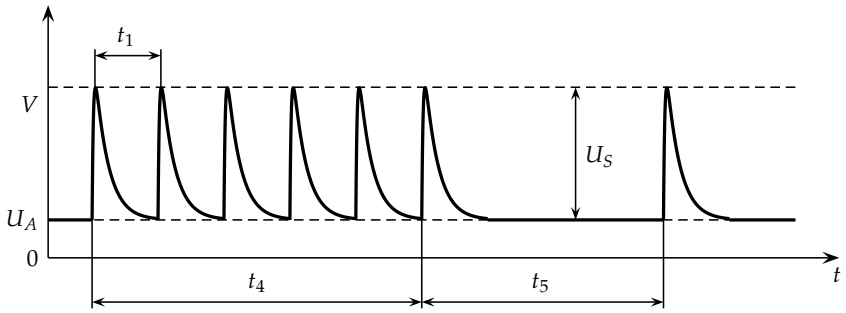

Single Pulse

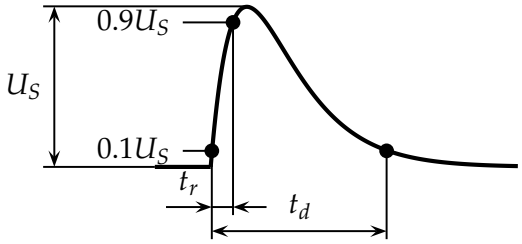

Figure 2.9: Test pulse 3b

Parameters	Nominal $12V$ system	Nominal $24V$ system
U_S	$75V \ldots 150V$	$150 \ldots 300V$
R_i	50Ω	
t_d	$150ns \pm 45ns$	
t_r	$5ns \pm 1.5ns$	
t_1	$100\mu s$	
t_4	$10ms$	
t_5	$90ms$	

Table 2.5: Parameters for Test Pulse 3b

2.4 Ideal Wave Forms

In (3) a mathematical model for the EFT voltage source for fast transient testing is given.
This model can be easily simulated in LTspice as an *Arbitrary Behavioural Voltage Source, ABVS*. In (3) the calculation for the double exponential pulse with the pulse width t_d from 50% to 50% of the signal amplitude is given. Since the automotive test pulses always have the pulse duration t_d from 10% to 10% of the amplitude, the algorithm had to be adjusted to get the parameters for automotive test pulses. The calculated parameters for Test Pulse 3b are:

$$\begin{aligned} V_{normed} &= k\left(e^{-\frac{t}{\alpha}} - e^{-\frac{t}{\beta}}\right) \\ &= 1.24\left(e^{-\frac{t}{61.65n}} - e^{-\frac{t}{3.324n}}\right) \end{aligned}$$

Figure (2.10) shows the simulated example of the Test Pulse. the rise time t_r is $5ns$ and the pulse width t_d is $150ns$

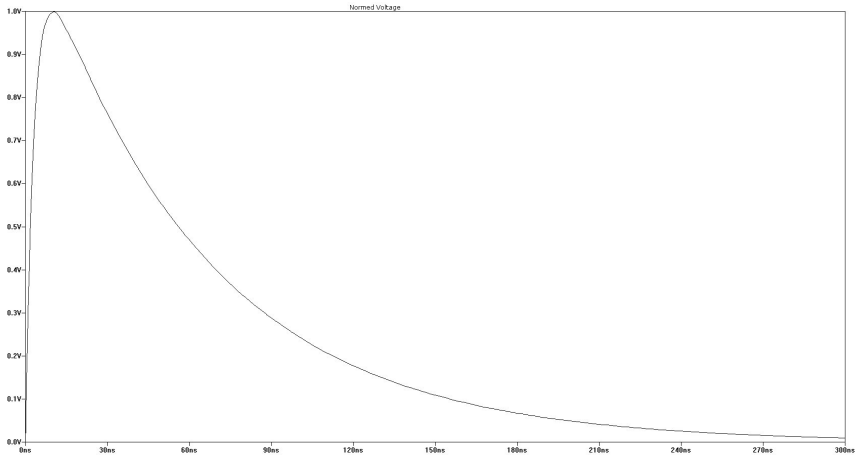

Figure 2.10: Ideal Waveform

3 Cable Theory

The HV- cables used for modeling the simulation setup have a coaxial- like structure. Therefore a short explanation of deriving the per unit length parameters is given.
For more detailed explanation it is referenced to (4) - (7).

3.1 External Parameters

First, the main characteristic properties of a coax cable are deduced. This parameters are only dependent on the geometry of the cable and the characteristics of the dielectric material. The external parameters are not dependent on the frequency of the alternating electric current and therefore apply at any frequency.

Capacitance

The capacitance is calculated by having a given charge (ΔQ) that is uniformly distributed over the outside surface of the inner conductor and an equal and opposite charge uniformly distributed on the inside surface of the outside conductor.
By placing the charge on the inner conductor, the electric flux density between inner and outer conductor can be calculated at any point r with $a < r < b$ since the charge distributions are uniformly around the conductor regardless of the conductor separations.
The Gaussian surface in the form of a cylinder with radius r and length Δl is used, that is concentric to the inner conductor.

Figure (6.9) illustrates the cable dimension in the longitudinal diametrical plane and figure (6.10) shows the electric field distribution in a coaxial cable.

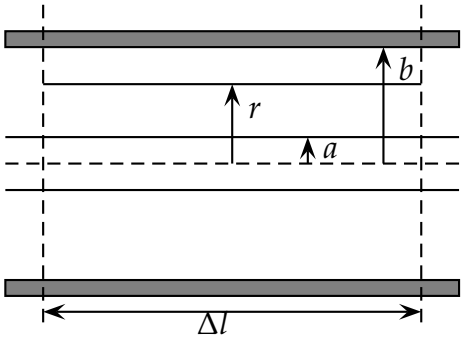

Figure 3.1: Cable Geometry

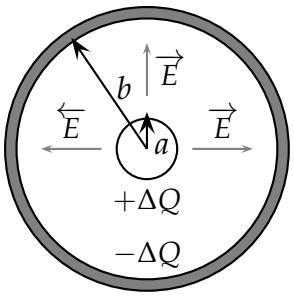

Figure 3.2: Electric Field

The radial electric flux density D_r:

$$D_r = \frac{\Delta Q}{\Delta l}\frac{1}{2\pi r} = \frac{\rho l}{2\pi r} \quad \left[C/m^2\right] \tag{3.1}$$

With:

Δl	length of the cable element
ΔQ	total charge
ρl	uniformly distributed charge density over the line length Δl

The space between inner and outer conductor is filled with a dielectric with some permittivity ϵ' and therefore the electric field E_r is derived:

$$E_r = \frac{D_r}{\epsilon'} = \frac{\rho l}{2\pi\epsilon' r} \quad [V/m] \tag{3.2}$$

The potential difference V_{ab} between two conductors:

$$\begin{aligned} V_{ba} &= \int_b^a -E_r \mathrm{dr} \quad [V] \\ V_{ab} &= \int_a^b E_r \mathrm{dr} = \int_a^b \frac{\rho l}{2\pi\epsilon' r} dr = \frac{\rho l}{2\pi\epsilon'} \ln\left(\frac{b}{a}\right) \quad [V] \end{aligned} \tag{3.3}$$

The capacitance between the two conductors of the coaxial cable over the length Δl is:

$$\Delta C = \frac{\Delta Q}{V_{ab}} \tag{3.4}$$

So the capacitance per unit length can be evaluated as:

$$C = \frac{\Delta C}{\Delta l} = \frac{\frac{\Delta Q}{\Delta l}}{V_{ab}} \ldots \text{with } \frac{\Delta Q}{\Delta l} = \rho l \tag{3.5}$$

$$C = \frac{2\pi\epsilon'}{\ln\left(\frac{b}{a}\right)} \quad [F/m] \tag{3.6}$$

Shunt Conductance

The conductance per unit length can be easily calculated from the formula of the capacitance from equation (3.6).

$$G = \frac{\sigma}{\epsilon'} C = \frac{2\pi\sigma}{\ln\left(\frac{b}{a}\right)} \quad [S/m] \tag{3.7}$$

The conductances describes the dielectric losses. Since insulators with good dielectric properties are used, it is usually very small.
Another way to derive the conductance is to calculate the electric field E_r, see equation (3.2), then calculating the total current by integrating the current density $J = \sigma E$ over the the cross section area of the cable:

$$I = \int_{\phi=0}^{2\pi} \sigma E r \mathrm{d}\phi = \frac{\sigma \rho_l}{2\pi\epsilon'} 2\pi \quad [A] \tag{3.8}$$

The current divided by the potential difference, equation (3.3), is the wanted conductance:

$$G = \frac{2\pi\sigma}{\ln\left(\frac{b}{a}\right)} \quad [S/m] \tag{3.9}$$

Inductance

The external inductance L_{ext} describes the linkage of the magnetic flux between the center conductor and the space between the inner and outer conductor of the line. In the inner conductor, the total current I flows longitudinally in one direction and in the outer conductor flows an equal current, but in the opposite direction, illustrated in figures (3.3) and (3.4).

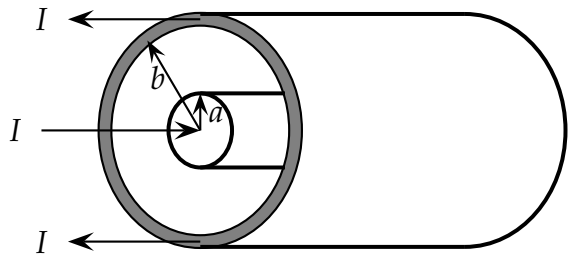

Figure 3.3

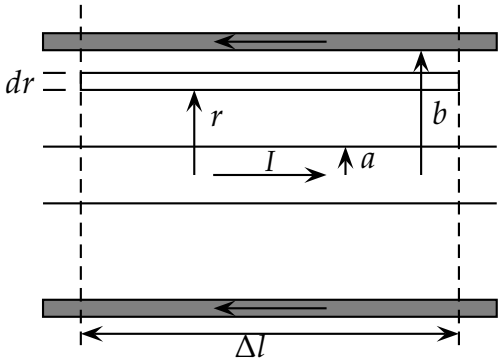

Figure 3.4: Longitudinal cross section

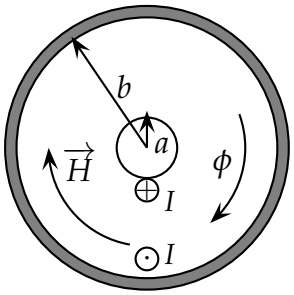

Figure 3.5: Cross section

The line is symmetric and the currents are uniformly distributed. The magnetic flux lines , that are produced by the current of the inner conductor, are concentric circles in the space between the inner and outer conductors, depicted in figure (3.5).
The flux density B at any point in the space between the conductors is:

$$B = \mu'_m H = \frac{\mu'_m I}{2\pi r} \quad [T] \tag{3.10}$$

Therefore the total flux of the center conductor in the space between the inner and outer conductor for Δl is:

$$\Delta\phi = \Delta l \int_a^b \frac{(\mu'_m I)}{2\pi r} dr = \frac{1}{2\pi} \Delta l \mu'_m \ln\left(\frac{b}{a}\right) \tag{3.11}$$

The per unit length external inductance L_{ext} is defined as the external flux linkage per unit length per unit current.

$$L_{ext} = \frac{1}{I\Delta l}\Delta\phi = \frac{\mu'_m}{2\pi} \ln\left(\frac{b}{a}\right) \quad [H/m] \tag{3.12}$$

The permeability always has the value for free space:
$\mu'_m = \mu_0 = 4\pi \cdot 10^{-7}\,[H/m]$.

3.2 Internal Parameters

This parameters are related to the magnetic field inside the conductors and are a function of the frequency. Figures (3.6) and (3.7) illustrate the current flow distribution in a conductor at low respectively high frequencies. The phenomenon at high frequencies is also called ”skin effect”.

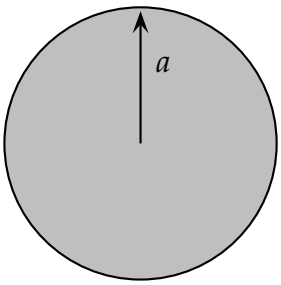

Figure 3.6: Low Frequencies (DC)

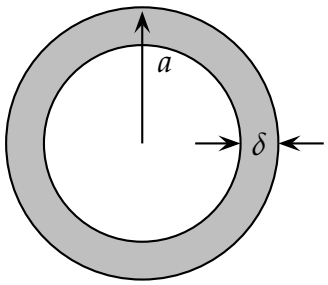

Figure 3.7: High Frequencies (AC)

Skin Effect

At higher frequencies the alternating current is not distributed over the whole surface anymore. It is concentrated in a ring concentric to the center, between the outer surface of the conductor and the skin depth δ. The effective resistance increases with higher frequencies and is proportional to $\sqrt{f}$ and the effective internal inductance decreases proportional to $\sqrt{f}$.

$$\delta = \frac{1}{\sqrt{\pi f \mu \sigma}} \tag{3.13}$$

Internal Inductance

Internal Inductance at low Frequencies

Figure (3.8) depicts the magnetic flux density B internal of the wire. The current flow distribution is like in figure (3.6).

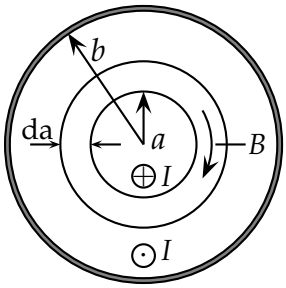

Figure 3.8: Cross Section

The magnetic flux density B internal of the wire:

$$B = \frac{\mu_0}{2\pi a} I \left(\frac{\pi a^2}{\pi b^2} \right) = \frac{\mu_0 I a}{2\pi b^2} \quad a < b \tag{3.14}$$

The total flux for a circle with radius a and thickness da:

$$\mathrm{d}\psi = \frac{\mu_0 I a}{2\pi b^2} \ \mathrm{da} \tag{3.15}$$

This flux only links a part of the total wire current $I\frac{\pi a^2}{\pi b^2}$ and this results to the flux linkage for the circle:

$$\mathrm{d}\psi = \frac{\mu_0 I a}{2\pi b^2}\frac{a^2}{b^2}\ \mathrm{da} = \frac{\mu_0 I a^3}{2\pi b^4}\ \mathrm{da} \tag{3.16}$$

The total flux linkage per unit length :

$$\psi = \int_{r=0}^{b} \frac{\mu_0 I a^3}{2\pi b^4}\ \mathrm{da} = \frac{\mu_0 I}{8\pi} \tag{3.17}$$

And the per unit length inductance at low frequencies is:

$$L_{int,dc_a} = \frac{\mu_0}{8\pi} \quad [H/m] \tag{3.18}$$

The per unit length value for the internal inductance is about $50\,[nH/m]$ and usually this is small compared to the external inductance.
The inductance in the sheath is calculated like for a circular tubular conductor:

$$L_{int,dc_{bc}} = \frac{\mu_0}{8\pi}\frac{1-4\left(\frac{b}{c}\right)^2+3\left(\frac{b}{c}\right)^3+4\left(\frac{b}{a}\right)^4\ln\left(\frac{c}{b}\right)}{\left[1-\left(\frac{b}{c}\right)^2\right]^2}\,[H/m] \tag{3.19}$$

The total p.u.l. inductance at low frequencies:

$$L = L_{ext} + L_{int,dc_a} + L_{int,dc_{bc}} \tag{3.20}$$

Where the external inductance L_{ext} represents the biggest part of the total value.

Internal Inductance at high Frequencies

For higher frequencies the internal inductance L_{int} will tend to be zero since the current will reside on the surface of the wire and therefore no internal current is linked by the field, as in depicted in figure (3.7).

$$\begin{aligned} L_{int,hf} &= \frac{2\delta}{a} L_{int,dc} \\ &= \frac{1}{4\pi a}\sqrt{\frac{\mu}{\pi\sigma}}\frac{1}{\sqrt{f}} \qquad [H/m] \end{aligned} \tag{3.21}$$

The total p.u.l. inductance at high frequencies:

$$L = L_{ext} + L_{int,hf} \qquad [H/m]$$

The internal inductance approaches very small values and the external inductance is the dominating part.

$$L = L_{ext} \qquad [H/m] \tag{3.22}$$

Resistance

Resistance at low Frequencies

At lower frequencies the current fills the inner and outer conductors of the cable completely. In this case the value of R_{dc} can be evaluated:

$$R_{dc} = \frac{1}{\sigma\pi a^2} + \frac{1}{\pi\sigma\left[(b+t)^2 - b^2\right]} \qquad [\Omega/m] \tag{3.23}$$

Where σ is the metal conductivity , a is the wire radius, b is the inner radius of the the outer conductor and t is the thickness of the outer conductor.

Resistance at high Frequencies

Resistance for the inner conductor with radius a:

$$R_i = \frac{1}{2\pi a \delta \sigma} \tag{3.24}$$

Resistance for the outer conductor with radius b:

$$R_o = \frac{1}{2\pi b \delta \sigma} \tag{3.25}$$

The total resistance is the sum of both the inner and the outer resistance since the current flows in series through this resistances.

$$R_{hf} = \frac{1}{2\pi \delta \sigma} \tag{3.26}$$

Applying equation (3.13) for the skin effect this leads to:

$$R_{hf} = \frac{1}{2}\sqrt{\frac{\mu}{\pi\sigma}}\sqrt{f}\left[\frac{1}{a} + \frac{1}{b}\right] \quad [\Omega/m] \tag{3.27}$$

3.3 Multi-Conductor Transmission Lines

This section gives a short overview about multi-conductor transmission lines (7) that were used for different simulation setups.

Method of Images

This method is used to solve electrostatic problems by replacing elements with "mirror" charges. The mirror charges replicate the boundary conditions of the problem.
For example, there is a point charge Q at distance h above the ground plane. To simplify the problem, the infinite plane is replaced by a point charge $-Q$ at distance h under the surface of the previous plane. The principle is displayed in figure (3.9).
The charge $-Q$ is also called the image of the positive charge.
Currents can be mirrored in the exact same manner. The fields above the ground plane remain identical.

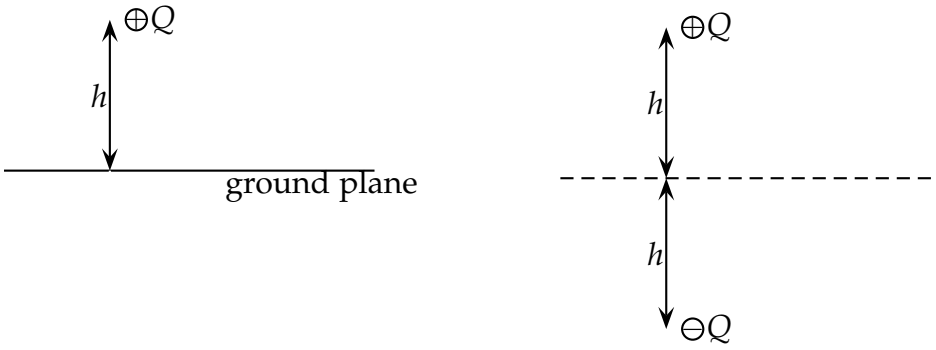

Figure 3.9: Method of Images for Point Charge

Parallel Cables above an infinite conducting Ground Plane

To calculate the self and mutual inductances of n-wires above a ground plane the *method of images* is used.

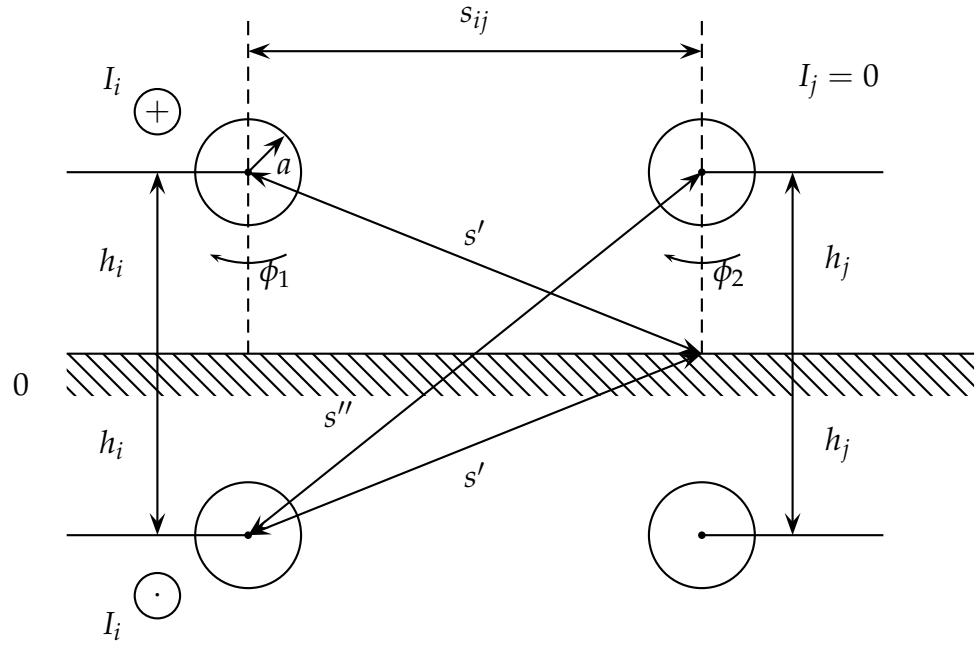

Self inductance of a wire over a ground plane:

$$\begin{aligned} L_{ii} =& \frac{\phi_i}{I_i}\Big|_{I_1=\cdots I_{i-1}=I_{i+1}=\cdots I_j=0} \\ =& \frac{\mu}{2\pi}\ln\left(\frac{h_i}{a}\right) + \frac{\mu}{2\pi}\ln\left(\frac{2h_i}{hi}\right) \\ =& \frac{\mu}{2\pi}\ln\left(\frac{2h_i}{a}\right) \quad [H/m] \end{aligned} \tag{3.28}$$

The mutual inductance between wires over the ground plane:

$$\begin{aligned} L_{ij} =& \frac{\phi_j}{I_i}\Big|_{I_1=\cdots I_{i-1}=I_{i+1}=\cdots I_j=0} \\ =& \frac{\mu}{2\pi}\ln\left(\frac{s'}{s_{ij}}\right) + \frac{\mu}{2\pi}\ln(\frac{s''}{s'}) \\ =& \frac{\mu}{2\pi}\ln\left(\frac{s''}{s_{ij}}\right) = \frac{\mu}{2\pi}\ln\left(\frac{\sqrt{s_{ij}^2+4h_ih_j}}{s_{ij}}\right) \\ =& \frac{\mu}{4\pi}\ln\left(1+\frac{4h_ih_j}{s_{ij}^2}\right) \\ & h_i = h_j = h \Rightarrow \\ L_{ij} =& \frac{\mu}{4\pi}\ln\left(1+\frac{4h^2}{s_{ij}^2}\right) \quad [H/m] \end{aligned} \tag{3.29}$$

Parallel Cables without infinite conducting Ground Plane

The self capacitance and inductance of the coax cables are calculated like in equations (3.6) and (3.12), for the external capacitance and external inductance, since the shield is the return conductor.

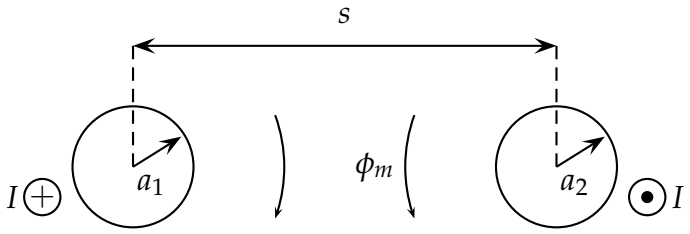

Figure 3.10: Cross section- parallel wires

The mutual inductance is:

$$\begin{aligned} L_m =& \frac{\phi_m}{I} \\ \phi_m =& \frac{\mu_0}{2\pi} I \left[\ln\left(\frac{s-a_2}{a_1}\right) + \ln\left(\frac{s-a_1}{a_2}\right) \right] \\ =& \frac{\mu_0}{2\pi} \ln\left(\frac{(s-a_1)(s-a_2)}{a_1 a_2}\right) \\ & a_1 = a_2 \Rightarrow \frac{\mu_0}{2\pi} I \ln\left(\frac{(s-a)^2}{a^2}\right) \\ & s >> a \Rightarrow \frac{\mu_0}{2\pi} I \ln\left(\frac{s^2}{a^2}\right) \Rightarrow \\ L_m =& \frac{\mu_0}{2\pi} \ln\left(\frac{s^2}{a^2}\right) \quad [H/m] \end{aligned} \tag{3.30}$$

Calculation of the Capacitance Matrix

The inductance matrix has the form of:

$$L = \begin{pmatrix} L_{11} & L_{12} & \cdots & L_{1i} \\ L_{12} & L_{22} & \cdots & L_{2i} \\ \vdots & \vdots & \ddots & \vdots \\ L_{1i} & L_{2i} & \dots & L_{ii} \end{pmatrix} \tag{3.31}$$

With L_{ii} are the self inductances of the wires and $L_{ij} = L_{ji}$, with $i \neq j$ are the mutual inductances.

The capacitance matrix then is derived from the inductance matrix:

$$C = \epsilon_0 \mu_0 L^{-1} \tag{3.32}$$

The capacitance matrix has the form of:

$$C = \begin{pmatrix} \sum_{j=1}^{i} c_{1j} & -c_{12} & \cdots & -c_{1i} \\ -c_{12} & \sum_{j=1}^{i} c_{2j} & \cdots & -c_{2i} \\ \vdots & \vdots & \ddots & \vdots \\ -c_{1i} & -c_{2i} & \cdots & \sum_{j=1}^{i} c_{ij} \end{pmatrix}$$

4 Cable Models

The specifications for modeling the cables are taken for the HV-cables from COROPLAST.
The cable model is :
COROPLAST, $FHLR2GCB2G$, $35mm^2$ for 600V/900V.

The nominal cable parameters are:

External Inductance L_{ext}	$100nH/m$
External Capacitance C_{ext}	$600pF/m$
Impedance	10Ω
DC resistance for the conductor $R_{dc_{inner}}$	$0.527m\Omega/m$
DC resistance for the shielding $R_{dc_{outer}}$	$0.035\Omega/m$.

1 . . . CORE
stranded bare copper
2 . . . CORE INSULATION
silicon rubber
wall thickness $\geq 0.64mm$
3 . . . SHIELD
tinned copper
4 . . . OUTER SHEATH
silicon rubber
wall thickness $\geq 0.8mm$

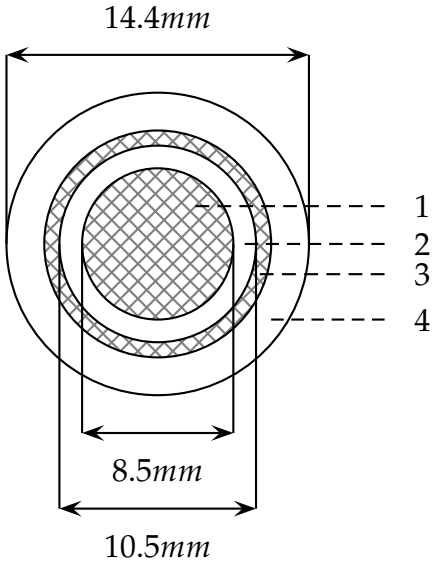

The following two skin effect models have been selected, because they are well functioning for circuit simulators like LTSpice.

4.1 Skin Effect Model: BIDYUT and WHEELER

In (**8**) the idea is to think that the conductor is composed of concentric shells. At low frequencies the current is distributed over all the shells and the internal resistance is at its minimum and the internal inductance has its maximum value. When the frequency increases, the inner shells gradually turn off because of the magnetic field inside the conductor. The outer shells remain active. For this reason the internal resistance increases and the internal inductance decreases.
This behavior is modeled by parallel branches and every branch is a serial connection of a resistance and an inductance, as illustrated in figure (4.1).

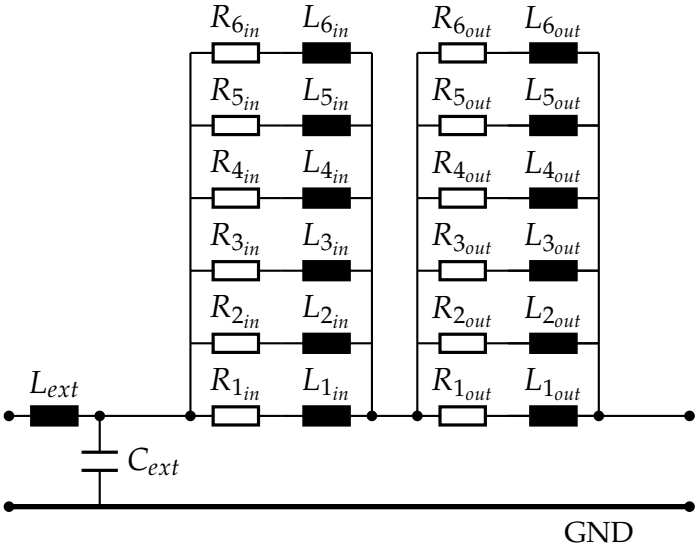

Figure 4.1: Circuit Model for Skin Effect

The number of branches used for the model is dependent on the bandwidth. Every added branch extends the range of validity for an additional decade of the frequency.

The parameters are calculated as followed:

$$\begin{aligned} R_n &= R_{dc} x^{n-1} \\ L_n &= \frac{L_{dc}}{x^{n-1}} \\ x &= \sqrt{10} \end{aligned} \tag{4.1}$$

The starting values for R_1 and L_1 for the iterative process for different scopes of validity for the bandwidth can be seen in table (4.1).
With six branches the model is valid from $1kHz$ up to $1GHz$ and as starting values the 6^{th} entity is taken.

Number of branches	R_1	L_1
1	R_{dc}	L_{dc}
2	1.32 R_{dc}	1.68 L_{dc}
3	1.42 R_{dc}	1.94 L_{dc}
4	1.45 R_{dc}	2.03 L_{dc}
5	1.457 R_{dc}	2.06 L_{dc}
$\rightarrow$ 6 $\leftarrow$	1.462 R_{dc}	2.07 L_{dc}

Table 4.1

4.2 Skin Effect Model: KIM and NEIKIRK

This method (**9**) proposes to model the skin effect with a four ladder circuit. The cross section of the conductor is divided into four concentric rings and every ring is described by one ladder. R_1 represents the ring on the outside. The resistances gradually proceed inside and R_4 represents the midmost part.
The concept can be seen in figure (4.2).

The ladder network for the inner and the outer conductor of the coaxial cable can be seen in figure (4.3).

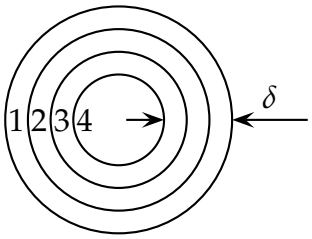

Figure 4.2: Partition of the Cross Section

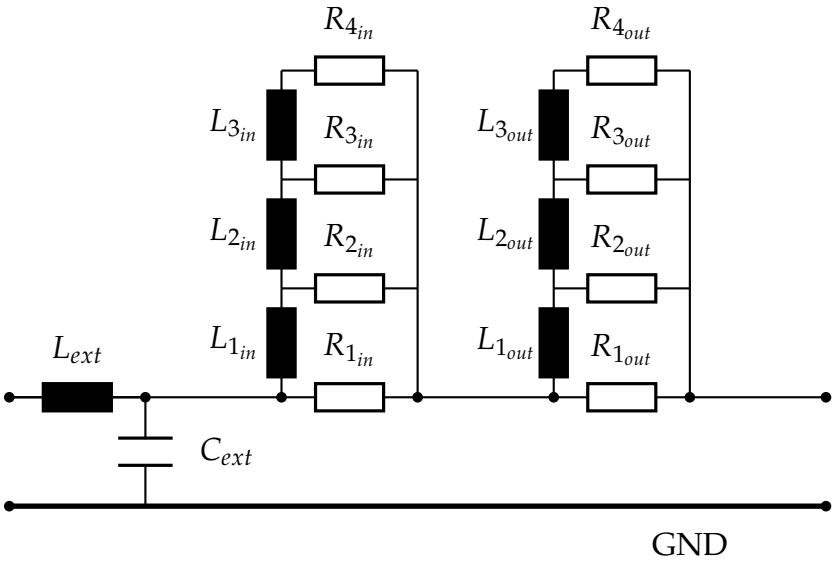

Figure 4.3: Four ladder network

Calculation of the parameters:

$$\begin{aligned} R_{n+1} &= \frac{R_n}{RR} \\ L_{n+1} &= \frac{L_n}{LL} \end{aligned} \tag{4.2}$$

Starting parameters to gather R_1 and L_1:
First, the skin depth at the maximum desired frequency is derived:

$$\delta_{min} = \frac{1}{\sqrt{\pi f_{max} \mu \sigma}} \tag{4.3}$$

As proposed in (**9**) the best start values R_1 and L_1 are:

$$\begin{aligned} R_1 =& 0.53 \cdot \frac{\text{wire radius}}{\delta_{min}} R_{dc} = \alpha_R R_{dc} \\ L_1 =& 0.351 \cdot \frac{R_1}{R_{dc}} L_{int} = 0.351 \alpha_R \end{aligned} \tag{4.4}$$

The values for RR and LL are obtained from the following relations:

$$(RR)^3 + (RR)^2 + RR + (1 - \frac{R_1}{R_{dc}}) = 0 \tag{4.5}$$

$$(\tfrac{1}{LL})^2 + (1 + \tfrac{1}{RR})^2 \tfrac{1}{LL} + ([\tfrac{1}{RR}]^2 + \tfrac{1}{RR} + 1)^2 - \tfrac{L_{int}}{L_1}([1 + \tfrac{1}{RR}][(\tfrac{1}{RR})^2 + 1])^2 = 0 \tag{4.6}$$

4.3 Simulation Results

Number of Subsections

The number of lumped elements is dependent on the maximum frequency f_{max} for which the model should be still valid. The length of the subsection should be smaller than one-tenth of the wavelength λ:

$$\begin{aligned} \lambda = \frac{c}{f_{max}} &= \frac{3 \cdot 10^8 m/s}{1 \cdot 10^9 Hz} = 0.3m \\ \text{with } c \ldots &\text{ speed of light} \\ len \leq \frac{\lambda}{10} &= \frac{0.3m}{10} = 0.03m \\ sub \geq \frac{1m}{len} &= \frac{1m}{0.03m} = 33.33 \end{aligned} \tag{4.7}$$

For the simulation the number of subsections is 40. This model should be valid for more than 1 GHz.
The values for the external capacitance C_{ext} and the external inductance L_{ext} are calculated by the equations (3.6) and (3.12).

$$L_{ext} = \frac{\mu_0}{2\pi} \ln\left(\frac{c}{a}\right)$$
$$C_{ext} = \frac{2\pi\epsilon_0\epsilon_r}{\ln\left(\frac{c}{b}\right)}$$

The internal inductances are calculated by equations (3.18) and (3.19).

$$L_{int,dc_{bc}} = \frac{\mu_0}{8\pi} \frac{1 - 4\left(\frac{b}{c}\right)^2 + 3\left(\frac{b}{c}\right)^3 + 4\left(\frac{b}{a}\right)^4 \ln\left(\frac{c}{b}\right)}{\left[1 - \left(\frac{b}{c}\right)^2\right]^2}$$
$$L_{int,dc_a} = \frac{\mu_0}{8\pi}$$

The values for the DC resistances were taken from the data sheet of the cable.
Parameters for calculation of the skin effect models:

L_{ext}	$97nH$	
C_{ext}	$611pF$	
$L_{lf_{in}}$	$50nH$	Internal LF inductance of the inner conductor
$L_{lf_{out}}$	$16nH$	Internal LF inductance of the shield
$R_{dc_{in}}$	$0.527m\Omega$	DC resistance of the inner conductor
$R_{dc_{out}}$	0.0035Ω	DC resistance of the shield

Results for Bidyut and Wheeler

The model with six branches was chosen and therefore the starting values are as given in table (4.1):

$$R_{n_{in}} = 1.462 \cdot R_{dc_{in}} \cdot \sqrt{10}^{(n-1)} \qquad L_{n_{in}} = \frac{2.07 \cdot L_{lf_{in}}}{\sqrt{10}^{(n-1)}}$$

$$R_{n_{out}} = 1.462 \cdot R_{dc_{out}} \cdot \sqrt{10}^{(n-1)} \qquad L_{n_{out}} = \frac{2.07 \cdot L_{lf_{out}}}{\sqrt{10}^{(n-1)}}$$

The results for all six branches:

$R_{1_{in}}$:	$0.77m\Omega$	$L_{1_{in}}$:	$103.5nH$	$R_{1_{out}}$:	0.0051Ω	$L_{1_{out}}$:	$32.77nH$
$R_{2_{in}}$:	$2.44m\Omega$	$L_{2_{in}}$:	$32.7nH$	$R_{2_{out}}$:	0.0162Ω	$L_{2_{out}}$:	$10.36nH$
$R_{3_{in}}$:	$7.70m\Omega$	$L_{3_{in}}$:	$10.3nH$	$R_{3_{out}}$:	0.0512Ω	$L_{3_{out}}$:	$3.28nH$
$R_{4_{in}}$:	$24.40m\Omega$	$L_{4_{in}}$:	$3.3nH$	$R_{4_{out}}$:	0.1618Ω	$L_{4_{out}}$:	$1.04nH$
$R_{5_{in}}$:	$77.00m\Omega$	$L_{5_{in}}$:	$1.0nH$	$R_{5_{out}}$:	0.5117Ω	$L_{5_{out}}$:	$0.33nH$
$R_{6_{in}}$:	$244.00m\Omega$	$L_{6_{in}}$:	$0.3nH$	$R_{6_{out}}$:	1.6181Ω	$L_{6_{out}}$:	$0.10nH$

Figure (4.4) shows the results for 1 meter simulated cable with skin effect in comparison to figure(4.5) without skin effect.

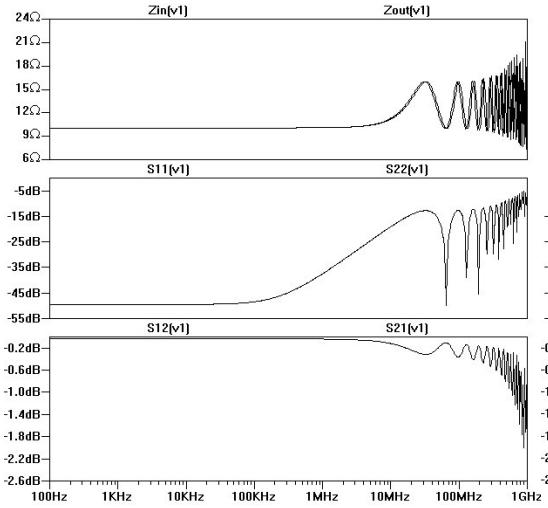

Figure 4.4: Skin Effect

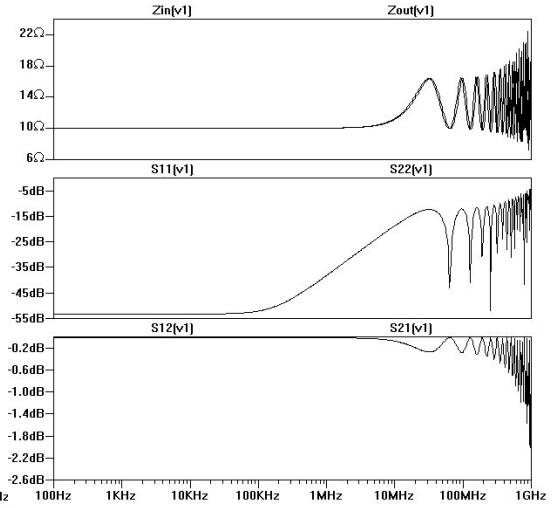

Figure 4.5: No Skin Effect

Results for Kim and Neikirk

This model was calculated for the minimum skin depth at a maximum frequency f_{max} of $1GHz$. Again with the start values from section(4.3). Following parameters were obtained:

$$\delta_{min} = \frac{1}{\sqrt{\pi f_{max} \mu_0 \sigma}} = 2.09\mu s$$

$$\begin{array}{lll} R_{1_{in}} = 0.568\Omega & RR_{in} = 9.9 & R_{n+1_{in}} = \frac{R_{n_{in}}}{9.9} \\ L_{1_{in}} = 0.0147nH & LL_{in} = 0.38 & L_{n+1_{in}} = \frac{L_{n_{in}}}{0.38} \end{array}$$

$$\begin{array}{lll} R_{1_{out}} = 6.124\Omega & RR_{out} = 11.7 & R_{n+1_{out}} = \frac{R_{n_{in}}}{11.7} \\ L_{1_{out}} = 0.287nH & LL_{out} = 0.35 & L_{n+1_{out}} = \frac{L_{n_{out}}}{0.35} \end{array}$$

Figure (4.6) shows the results for $1m$ simulated cable with skin effect modeled in comparison to figure (4.7) without skin effect.

Results for $1GHz$

$R_{1_{in}}$:	$568.00m\Omega$	$L_{1_{in}}$:	$0.0147nH$	$R_{1_{out}}$:	6.124Ω	$L_{1_{out}}$:	$0.287nH$
$R_{2_{in}}$:	$57.40m\Omega$	$L_{2_{in}}$:	$0.0381nH$	$R_{2_{out}}$:	0.5236Ω	$L_{2_{out}}$:	$0.381nH$
$R_{3_{in}}$:	$5.80m\Omega$	$L_{3_{in}}$:	$1.006nH$	$R_{3_{out}}$:	0.0448Ω	$L_{3_{out}}$:	$0.241nH$
$R_{4_{in}}$:	$0.59m\Omega$			$R_{4_{out}}$:	0.0038Ω		

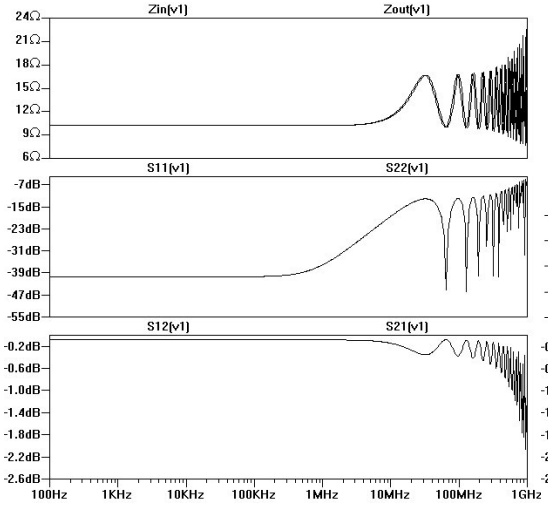

Figure 4.6: Skin Effect

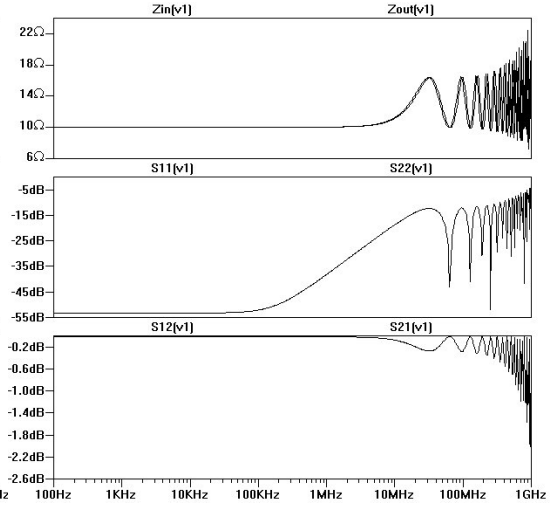

Figure 4.7: No Skin Effect

5 Capacitive Coupling Clamp

Due to internal and external sources, disturbances can couple into the main power supply of vehicles. The disturbances inject through signal- and control lines into the peripherals and can affect their correct functionality.
The capacitive coupling clamp (CCC) is used to test fast transient immunity of these components, regarding the international standard ISO $7637-3$, (**10**). The schematic test setup is shown in figure (5.1).

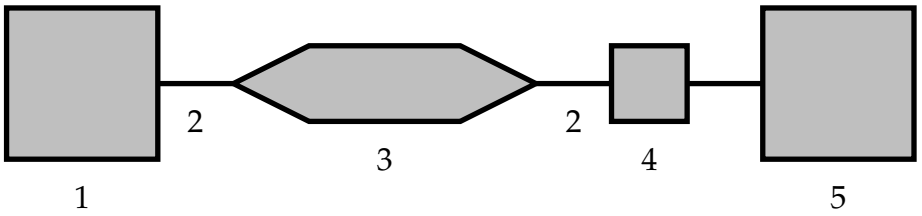

Figure 5.1: CCC- Test Setup

1 Impulse Generator
2 Cable with 50Ω characteristic impedance
3 Capacitive Coupling Clamp
4 50Ω attenuator
5 Oscilloscope, 50Ω

The impulses used for testing are mainly the Test Impulses 3a and 3b, whose characteristic waveforms have been explained in section (2.3). For this setup Test Pulse 3b is applied and it is modeled via the double exponential pulse as obtained in section (2.4). The advantage of this mathematical characterization is, that the pulse can be easily simulated as an Arbitrary Behavioral Voltage Source with the LTSpice simulator.

When leaving the coaxial connector open, instead of using the 50Ω attenuator, this setup is also valid for BURST testing regarding *IEC 61000-4-4*, for transient immunity testing.

Simulation Setup for the CCC

For the simulation setup, basically two parts have to be considered.
The first part is the wiring harness above the ground plane outside the clamp. The second part consists of the coupling clamp housing the cables. The cables itself have a characteristic impedance of 10Ω, the clamp and the impulse- generator have a characteristic impedance of 50Ω.
The principle is shown in figure (5.2)

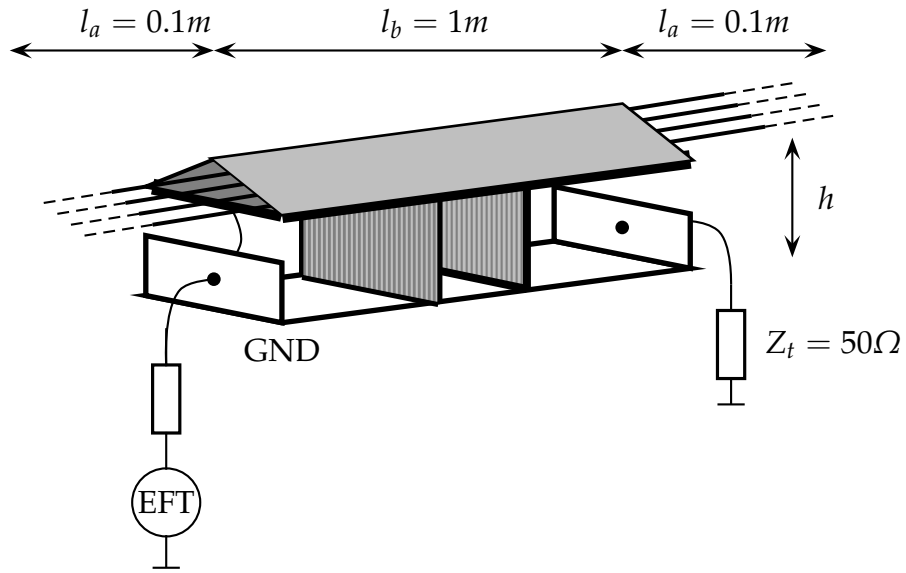

Figure 5.2: Clamp Setup

The length l_b of the clamp housing the cables is one meter, the length l_a of the cables outside the clamp is 10 centimeters and the height h above the ground plane for the whole setup is 10 centimeters.

5.1 Wires above Ground Plane

Figure (5.3) depicts the cross section of the parallel cables above the ground plane.

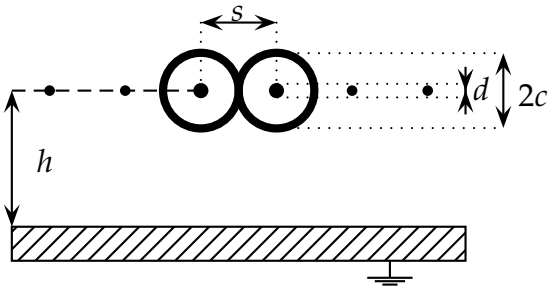

Figure 5.3: Cable over Ground Plane

For this arrangement the inductance matrix of i conductors is computed by applying equation (3.28) and equation (3.29).

$$L_{ii} = \frac{\mu_0}{2\pi} \ln\left(\frac{2h}{c}\right) \qquad i = 1, 2, ..., n \tag{5.1}$$

$$L_{ij} = L_{ji} = \frac{\mu_0}{4\pi} \ln\left(1 + \frac{4h^2}{s^2}\right) \qquad i, j = 1, 2, ..., n; i \neq j \tag{5.2}$$

h ... height of the conductors over the ground plane
s ... separation between the conductors
c ... radius of the outer conductor
since the assumption is a "thick" wire above ground

The capacitance matrix C is derived from L by $C = \mu_0 \epsilon_0 L^{-1}$. The separation distance between the wires and the ground plane is relatively large compared to the wire diameter. Therefore the insulation has an insignificant effect on the self capacitance values. However for the mutual capacitances it needs to be taken into account (**11**). Wires that are not adjoined have been neglected.

Therefore the capacitance matrix C is:

$$C_{ii} = C_{0ii} \qquad i = 1, 2, ..., n; \tag{5.3}$$

$$C_{ij} = C_{0ij}\epsilon_r \qquad i, j = 1, 2, ..., n; i \neq j \tag{5.4}$$

Figure (5.4) shows the per unit length model of the cables over the ground-plane.

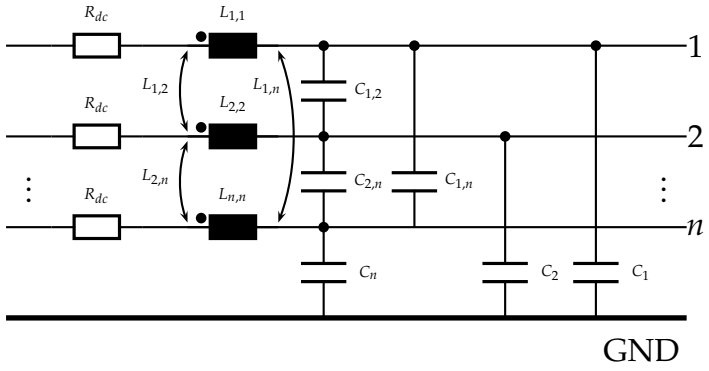

Figure 5.4: p.u.l. Parameters

5.2 Model of the Clamp housing Cables

The clamp is represented by the clamp inductance L_{clamp} of 400 $\left[\frac{nH}{m}\right]$ and the shunt capacitance C_{clamp} of 55 $\left[\frac{pF}{m}\right]$ in the ladder network (figure (5.5)). This values have been taken from (**11**).

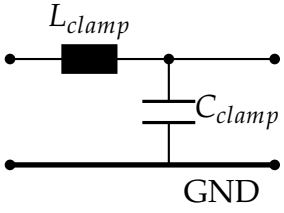

Figure 5.5

5.2.1 Conductors between parallel Ground Planes

Capacitance Calculation

Figure (5.6) illustrates the principle of this structure. Between the ground plates, that are assumed as reference conductors, n equally spaced parallel cables are placed.

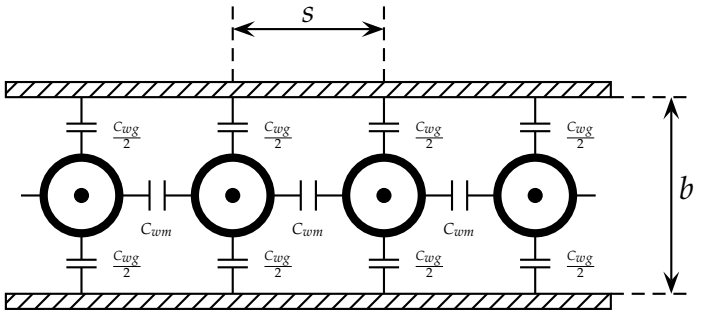

Figure 5.6

The explanation of the calculation of the self- and mutual capacitances is taken from (**12**) and (**13**).
The TEM propagation along the structure can be described in terms of two orthogonal modes, the even and the odd mode.
In the even mode all center conductors are at the same potential. All lines are driven by voltage generators with the same amplitude and phase.
In the odd mode adjacent center conductors are at equal but opposite signed potentials with respect of the ground planes.
The TEM modes have different characteristic impedances, that are related to the total static capacitances of the rods to ground. This total static capacitances are in relation with the mutual capacitance C_{wm} between adjacent rods, and the self capacitance C_{wg} of each rod to ground.

The total even mode capacitance between one rod and the two ground planes is:

$$C_{even} = C_{wg} \tag{5.5}$$

Total capacitance between one rod and the ground planes in odd mode:

$$C_{odd} = C_{wg} + 4C_{wm} \tag{5.6}$$

From this relations the self capacitances C_{wg} and mutual capacitance C_{wm} can be derived:

$$C_{wg} = C_{even} \tag{5.7}$$

$$C_{wm} = \frac{1}{4}(C_{odd} - C_{even}) \tag{5.8}$$

The normalized capacitances for the even and the odd mode are derived by the following calculations:

$$\begin{aligned}
\frac{\epsilon}{C_{odd}} &= \frac{1}{2\pi}\left|\ln\frac{\frac{\pi}{4}\frac{d}{b}}{\sqrt{1-\left(\frac{d}{2b}\right)^4}} - \frac{1}{2}\ln\left[1-\left(\frac{\frac{d}{b}}{2\left(\frac{c}{b}\right)}\right)^4\right] + 2\sum_{m=1}^{\infty}(-1)^m \ln\tanh m\frac{\pi}{2}\frac{c}{b}\right| \\
\frac{\epsilon}{C_{even}} &= \frac{1}{2\pi}\left|\ln\frac{\frac{\pi}{4}\frac{d}{b}}{\sqrt{1-\left(\frac{d}{2b}\right)^4}} + \frac{1}{2}\ln\left[1-\left(\frac{\frac{d}{b}}{2\left(\frac{c}{b}\right)}\right)^4\right] + 2\sum_{m=1}^{\infty}\ln\tanh m\frac{\pi}{2}\frac{c}{b}\right|
\end{aligned} \tag{5.9}$$

Inductance Calculation

The inductance matrix can be computed as in section (5.1), by calculating $L = \mu_0\epsilon_0 C^{-1}$. Nonadjacent wires have not been taken into account and

therefore the capacitance matrix has the form of:

$$C = \begin{pmatrix} C_{wg}+C_{wm} & -C_{wm} & 0 & \cdots & 0 \\ -C_{wm} & C_{wg}+2C_{wm} & -C_{wm} & \cdots & 0 \\ \cdots & \vdots & \vdots & \ddots & \vdots \\ 0 & \cdots & 0 & -C_{wm} & C_{wg}+C_{wm} \end{pmatrix}$$

5.2.2 Mutual Inductance between CCC and Cable

Figure (5.7) shows the cross section of the capacitive coupling clamp with cables inside.

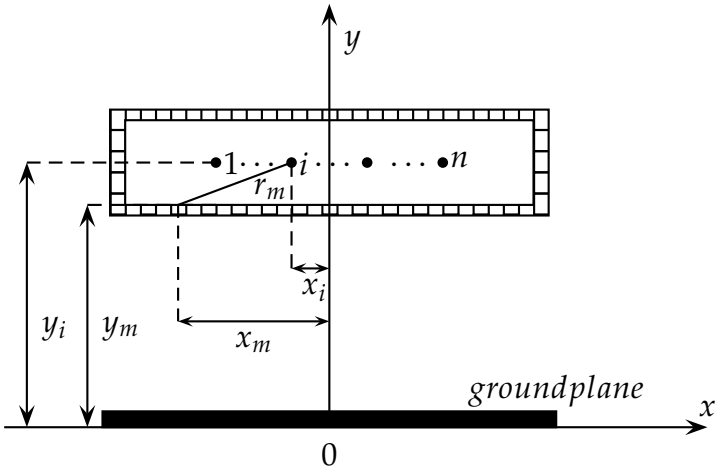

Figure 5.7: Cross Section of the CCC

The mutual inductances $L_{ai,clamp}$ are calculated via the Neumann integral: Calculation of the inductance for loops i and j is done by applying the Maxwell equation in integral form (**14**) and (**15**):

$$M_{ij} = \frac{1}{a_i a_j}\frac{\mu}{4\pi}\oint_i \int_{a_i} \oint_j \int_{a_j} \frac{dI_i \cdot dI_j}{r_{ij}} da_i da_j \tag{5.10}$$

The Neumann formula is given by:

$$M_{f_{12}} = \oint_i \oint_j \frac{dI_i \cdot dI_j}{r_{ij}} \tag{5.11}$$

Expression (5.10) can be simplified via the Neumann equation and this results too:

$$M_{ij} = \frac{1}{a_i a_j} \int_{a_i} \int_{a_j} M_{f_{12}} da_i da_j \tag{5.12}$$

Therefore the partial inductances can be written also in the following way:

$$M_{p_{km}} = \lim_{\substack{K\to\infty \\ M\to\infty}} \frac{1}{KM} \sum_{i=1}^{K} \sum_{j=1}^{M} L_{pf_{ij}} \tag{5.13}$$

Every of the n wires is assumed to be one filament, so $K = 1$ and the cross section of the clamp is subdivided in M filaments, as in (**11**).
This leads to the expression:

$$L_{wi_{clamp}} = \lim_{M\to\infty} \frac{1}{M} \sum_{m=1}^{M} L_{f_{im}}, i = 1, \ldots, N \tag{5.14}$$

With:

$$L_{f_{im}} = \frac{\mu}{4\pi} \ln\left(1 + \frac{4y_i y_j}{r_{im}^2}\right), i = 1, \ldots, N; m = 1, \ldots, M \tag{5.15}$$

$$r_{im} = \sqrt{(y_m - y_i)^2 + (x_m - x_i)^2}, i = 1, \ldots, N; m = 1 \ldots, M \tag{5.16}$$

To note that equation 5.15 is the calculation for the mutual inductance of n parallel wires above a ground plane and r_{im} is the distance between the two wires.

Transformation

The final model of the coupling clamp, as depicted in figure (5.9), is obtained by merging two different models. One model is the clamp housing the cable and the other is the model of the clamp itself.
This principle can be seen in figure (5.8).

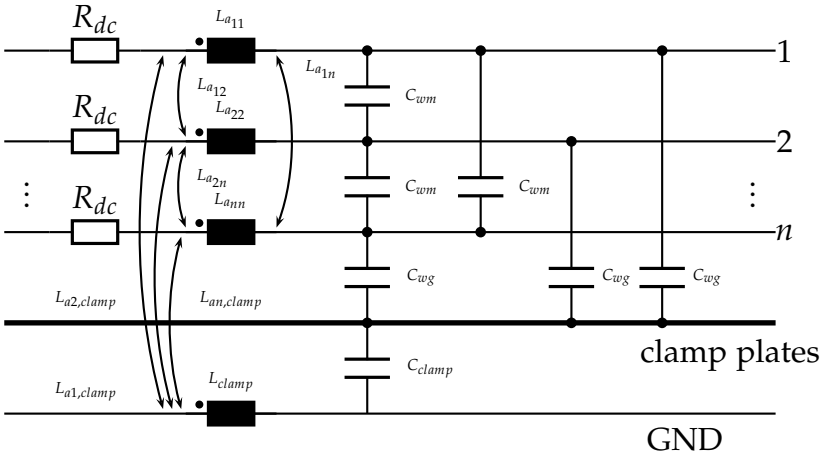

Figure 5.8: CCC housing cable- referenced to Clamp Plates

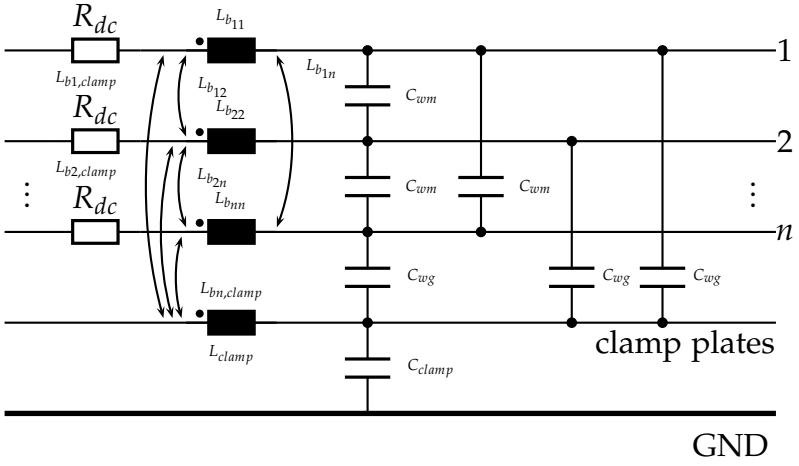

Figure 5.9: CCC housing Cables- referenced to Ground Plane

Mutual capacitances between the clamp and the cable have been neglected. The mutual inductances between the clamp and the wires have to be considered.

The n- dimensional vector of mutual inductances $L_{a,clamp}$ is:

$$L_{a,clamp} = \left[L_{a1,clamp}, \ldots, L_{an,clamp}\right]$$

The inductance matrix L_{wc} is the follwing $(n+1) \times (n+1)$ matrix:

$$L_{wc} = \begin{pmatrix} L_A & L_{a,clamp}^T \\ L_{a,clamp} & L_{clamp} \end{pmatrix}$$

The reference conductor of the circuit has to be be moved to the ground plane. How to define a return path is explained in (**16**). Therefore the final inductance matrix L_b of the system correclty referenced to groud is:

$$L_b = P^T L'_{wc} P$$

With L'_{cw} is the $(n+2) \times (n+2)$ inductance matrix

$$L'_{wc} = \begin{pmatrix} L_a & 0_{n,1} & L_{w,clamp}^T \\ 0_{1,n} & 0 & 0 \\ L_{w,clamp} & 0 & L_{clamp} \end{pmatrix}$$

P is a $(n+2) \times (n+1)$ Matrix, consisting of the $(n+1)$ identity matrix and its last row is -1:

$$P = \begin{pmatrix} \boldsymbol{I}_{(n+1)\times(n+1)} \\ \begin{pmatrix} -1 & -1 & \ldots \end{pmatrix}_{1\times(n+1)} \end{pmatrix}$$

6 Simulation of the Test Setup

Test Impuls 3b

For this simulation the test pulse $3b$, as described In section (2.4), is used. It is simulated in LTSpice via an Arbitrary Behavioral Voltage Source (ABVS). Its amplitude is set to 300V.

$$V_{test} = 300 \cdot 1.24 \left(e^{-\frac{t}{61.65n}} - e^{-\frac{t}{3.324n}} \right)$$

Number of Subsections

The cables used for this work are again the shielded cables from COROPLAST as described in chapter (4). The length of one subsection:

$$\lambda = \frac{c}{f_{max}}$$
$$len \leq \frac{\lambda}{10} \Rightarrow sub \geq \frac{1m}{len}$$

With c is the speed of light and λ is the wavelength. Each subsection hast the length of $0.1m$, so the model should be valid up to $285MHz$.

Parallel Cable above Ground Plane

The inductance calculation is for two parallel wires above a ground plane. The self inductances L_{ii} are calculated as in equation (3.28) and the mutual

inductances L_{ij} are derived from equation (3.29).

The parameters are:

h	height of the cable above ground	$100mm$
c	radius of the sheath	$6.8mm$
ϵ_r	permittivity	3

$$\begin{aligned} L_{11} = L_{22} &= \frac{\mu_0}{2\pi} \ln\left(\frac{2h}{c}\right) \\ &= 737.4 \quad nH/m \\ L_{12} = L_{21} &= \frac{\mu_0}{2\pi} \ln\left(1 + \frac{4h^2}{s^2}\right) \\ &= 224 \quad nH/m \end{aligned}$$

The coupling factor between the two cables is:

$$k = \frac{L_{12}}{\sqrt{L_{11}L_{12}}} = 0.83$$

The capacitance matrix is calculated as in equation (3.32).

$$C = \mu_0 \epsilon_0 L^{-1}$$

Therefore the mutual capacitances are:

$$\begin{aligned} C_{11} = C_{22} &= 104.2 \quad pF/m \\ C_{12}\epsilon_r = C_{21}\epsilon_r &= 45.5 \quad pF/m \end{aligned}$$

The schematics for the different types of the skin effect models can be seen in figure (6.1) and figure (6.2).

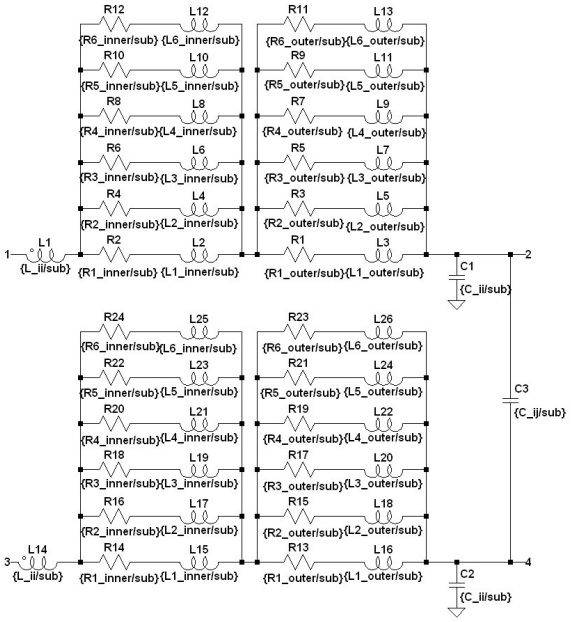

Figure 6.1: Skin Effect Wheeler

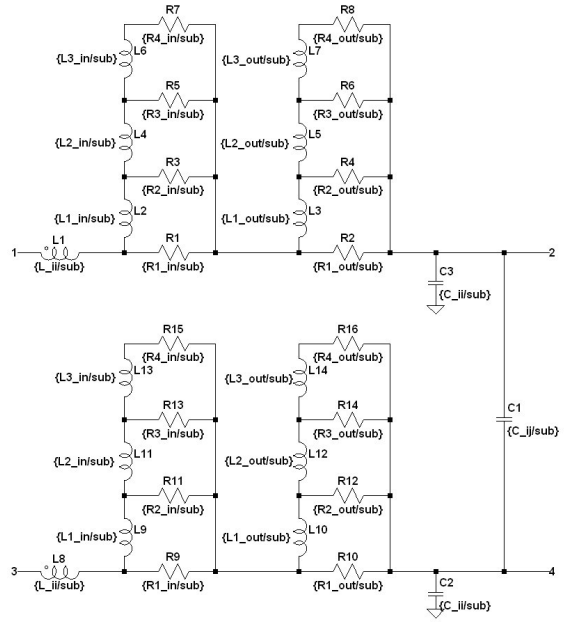

Figure 6.2: Skin Effect Neikirk

Clamp housing two parallel Cables

The parameters are:

h	height of the cable above ground	$100mm$
c	radius of the sheath	$6.8mm$
ϵ_r	permittivity	3
s	distance between the two cables	$20mm$
b	distance of the Clamp Plates	$30mm$

Conductors between parallel Ground Planes

The capacitances are calculated by equation (5.8). The resulting values and the capacitance matrix are:

$$\begin{aligned} C_g &= 104.2 \ \ pF/m \\ C_m &= 45.5 \ \ pF/m \\ \implies C &= \begin{pmatrix} 149.7pF & -45.5pF \\ -45.5pF & 149.7pF \end{pmatrix} \end{aligned}$$

Therefore the inductance matrix is:

$$L_a = \begin{pmatrix} 737.4nH & 224nH \\ 224nH & 737.4nH \end{pmatrix}$$

The mutual inductances between the cables and the clamp:

$$L_{a,clamp} = [124.4nH, 124.4nH]$$

The transformation matrix P:

$$P = \begin{pmatrix} 1 & 0 & 0 \\ 0 & 1 & 0 \\ 0 & 0 & 1 \\ -1 & -1 & -1 \end{pmatrix}$$

The matrix $L_{wc'}$:

$$L_{wc'} = \begin{pmatrix} 737.4nH & 224nH & 0 & 124.4nH \\ 224nH & 737.4nH & 0 & 124.4nH \\ 0 & 0 & 0 & 0 \\ 124.4nH & 124.4nH & 0 & 400nH \end{pmatrix}$$

After the transformation $L_b = P' L_{wc'} P$, the final results are:

Self- and mutual inductances of the cables:

$$\begin{aligned} L_{b_{11}} &= L_{b_{22}} &&= 888.6 \quad nH/m \\ L_{b_{12}} &= L_{b_{21}} &&= 375.2 \quad nH/m \end{aligned}$$

Coupling factor between the two cables:

$$k_2 = \frac{L_{b_{ij}}}{\sqrt{L_{b_{ii}} L_{b_{ij}}}} = 0.65$$

Mutual inductance between clamp and cable:

$$L_{b1_{clamp}} = L_{b1_{clamp}} = 275.6 \quad nH$$

Coupling factor between the clamp and the cable:

$$k_3 = \frac{L_{bi_{clamp}}}{\sqrt{L_{bi_{clamp}} L_{b_{11}}}} = 0.5$$

The schematics for the two models for one lumped element can be seen in figure (6.3) respectively in figure (6.4).

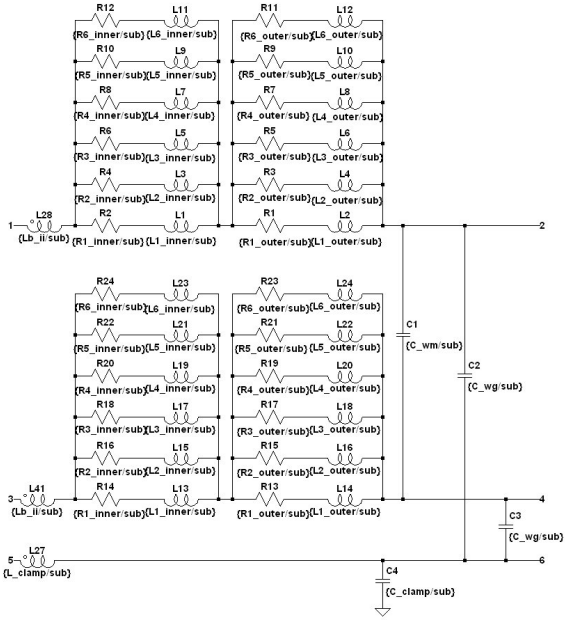

Figure 6.3: Skin Effect Wheeler

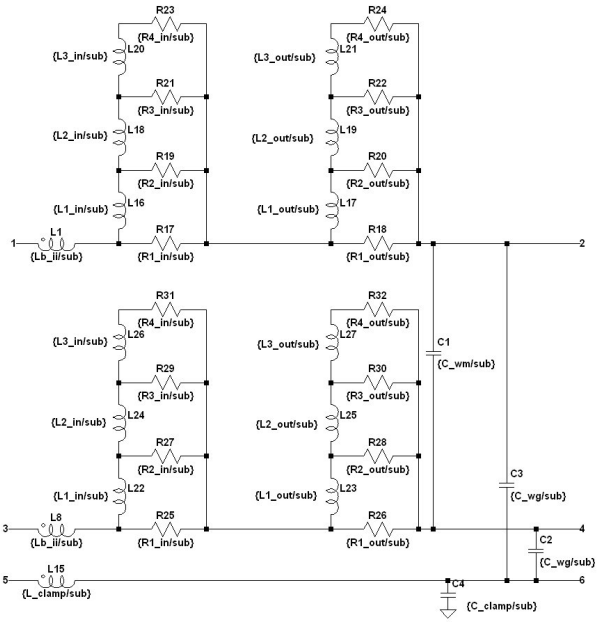

Figure 6.4: Skin Effect Neikirk

6.1 Simulation Results

Figure (6.5) illustrates the general setup. The ports C and D are terminated with the impedance of the cable, $Z = 10\Omega$.

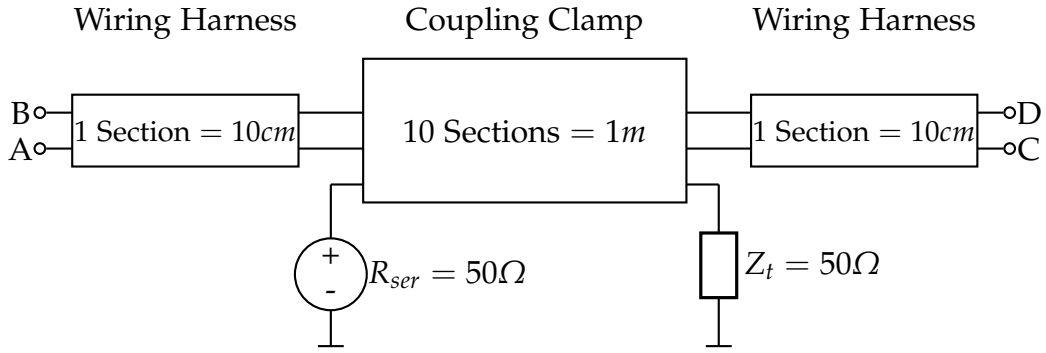

Figure 6.5: Simulation Setup

Result with Test Pulse 3b, Open Circuit Voltage of $300V$

Terminal A and B where left open to measure the voltage on the side of the device under test.
The value for both skin effect models was $169.7V$. The simulation results can be seen in figures (6.6) and (6.7).
Calculating the attenuation for the setup:

$$IL = 20\log\left(\frac{U_{out}}{U_{in}}\right) = 20\log\left(\frac{169.7V}{300V}\right) = -4.9dB \tag{6.1}$$

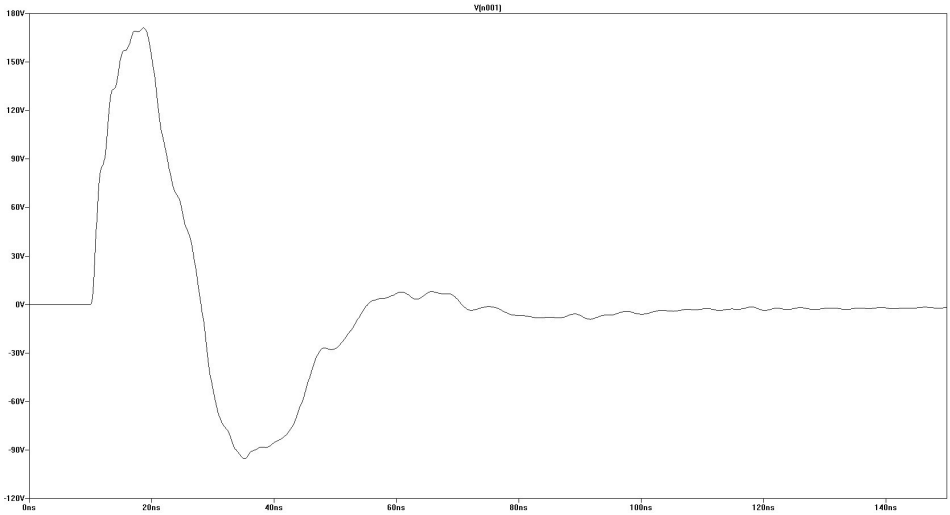

Figure 6.6: Bidyut and Wheeler

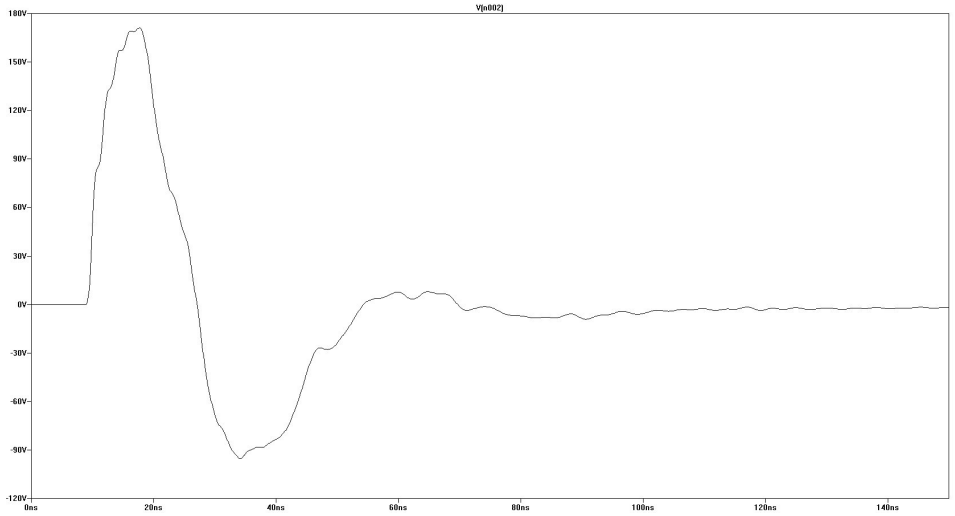

Figure 6.7: Kim and Neikirk

Figure 6.8 shows the simulated results without modeling the sin effect. Only the external parameters of the cable have been simulated. The results with and without the models are the same. There fore at this frequencies the modeling of the skin effect is not necessarily needed.

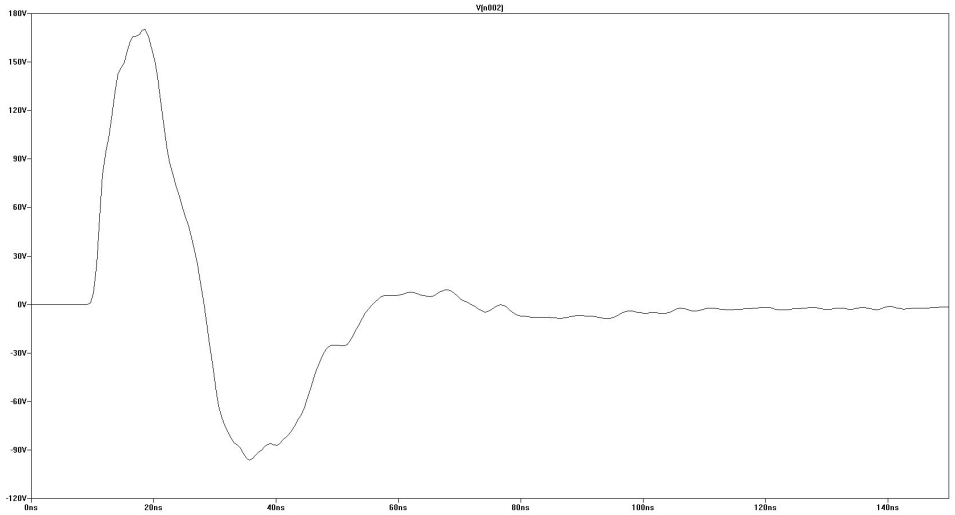

Figure 6.8: No Skin Effect modeled

Results for a $1nF$ Filter

Measured Values

This simulation was done with a $1nF$ filter at ports A and B. The resulting value was $16.6V$ for both models. The simulated results can be seen in figures (6.9) and (6.10).
The total attenuation is

$$IL_{total} = 20\log\left(\frac{U_{out}}{U_{in}}\right) = 20\log\left(\frac{16.6V}{300V}\right) = -25.2dB \qquad (6.2)$$

Calculated Values:

f_c	$3.18Mhz$	cut off frequency of the $1nF$ capacitor
f_{max}	$\frac{1}{2\pi 5ns} = 32.5Mhz$	maximum frequency of the signal

The cut off frequency of the capacitor is $3.18Mhz$ and since the maximum frequency f_{max} is more or less ten times the cut off frequency, the insertion loss of the filter is about $-20db$ at f_{max}.

The attenuation of the clamp setup is $-4.9dB$, as calculated in equation (6.1), for the frequency f_{max}.

Therefore the total attenuation of the setup is:

$IL_{total} = IL_{clamp} + IL_{filter} = -25dB.$

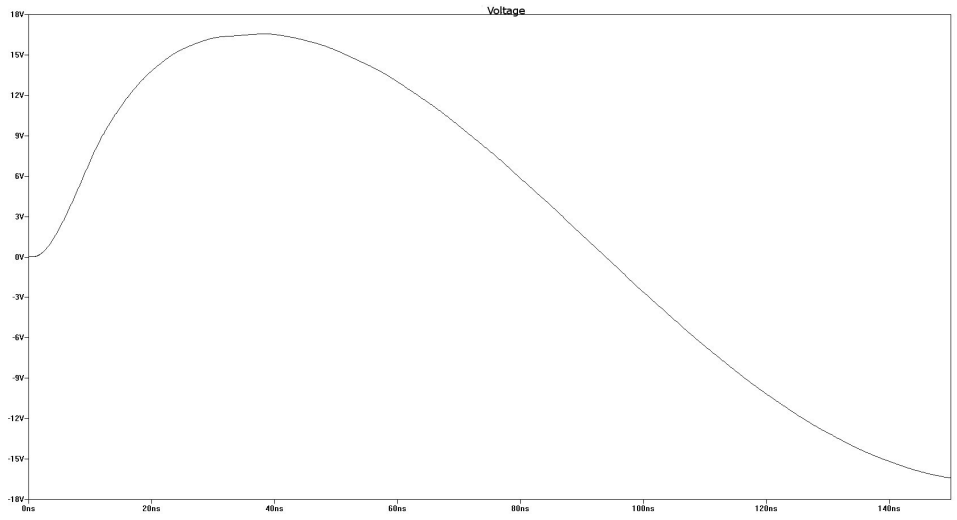

Figure 6.9: Bidyut and Wheeler : $1nF$ Filter

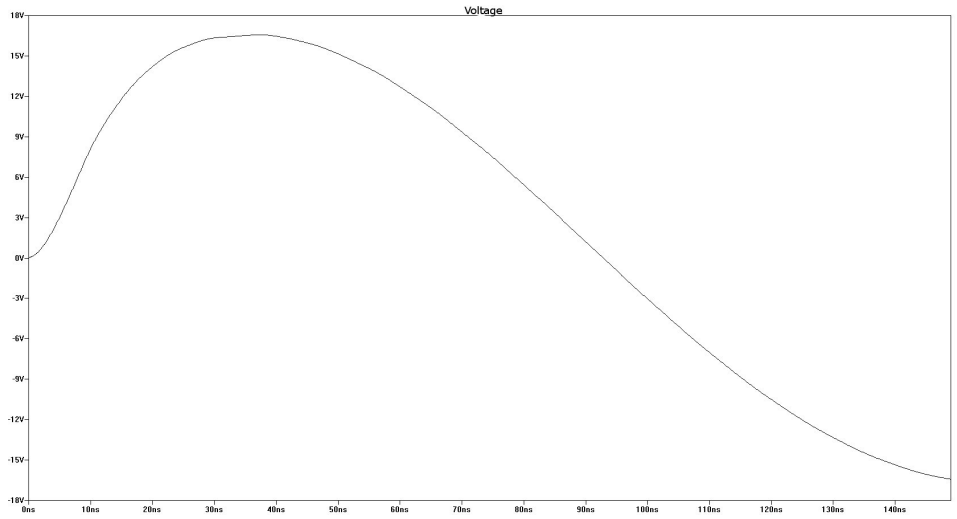

Figure 6.10: Kim and Neikirk: $1nF$ Filter

7 Conducted Disturbances- Electric Drive System

Two different simulation setups were modeled. The first setup is for simulating the conducted disturbances on the HV- cables, generated by the inverter. The principle is shown in figure (7.1).

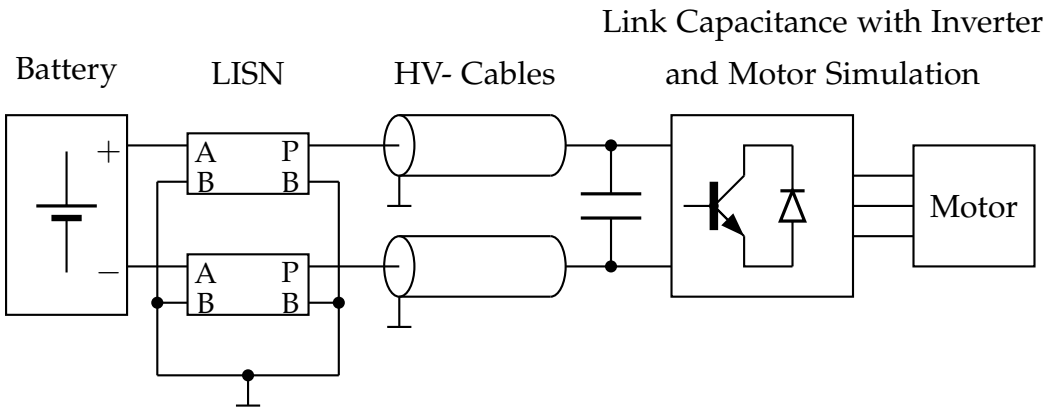

Figure 7.1: Test Setup 1

The aim of the second setup is to simulate the overall disturbances generated by the total electric drive system. The idea is to derive results that fit to more real conditions, without using the Line Impedance Stabilization Network (LISN), as demonstrated in figure (7.2).

In the following sections the main parts of the setup are explained and in section (7.5) the final results of the simulation are given.

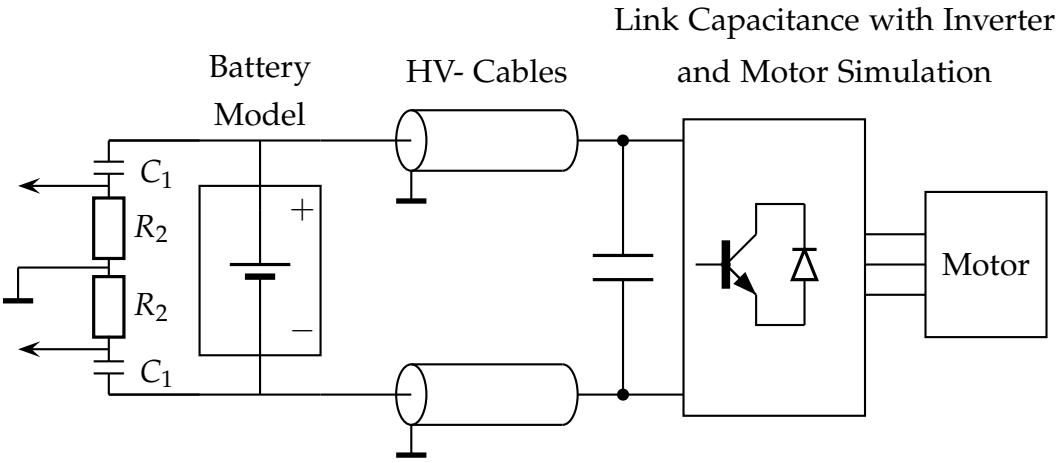

Figure 7.2: Test Setup 2

7.1 Battery Model

A battery module consists of several single battery cells, that are connected together to form the whole battery. Since there was no Lithium Ion battery for measurements available, the construction phase of the battery model is taken from (**17**).
In this reference, 35 battery cells of $3.7V$ were connected in series to achieve a battery voltage of $130V$.

The derived values by measurement and computation are:

Parameters for $130V$		
C_P	...	$20pF$
R_{DC}	...	1.06Ω
L_{HF}	...	$217.96nH$
C_{HF}	...	$10.4nF$

From the equivalent circuit diagram for a battery cell for high frequencies, as depicted in figure (7.3), the serial and parallel connections of the network elements are apparent.

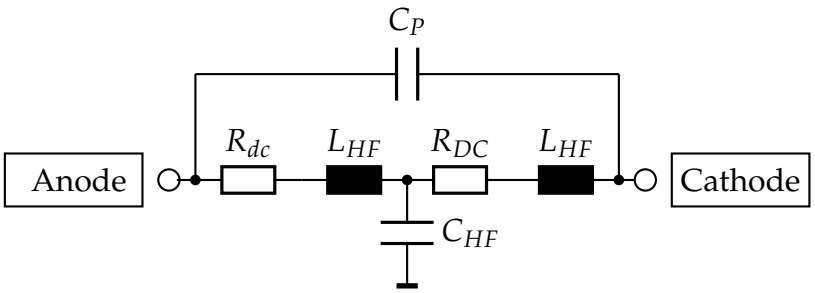

Figure 7.3: Battery Cell Principle for HF

Calculation of Parameters R_{DC}, L_{HF} and C_{HF}

From the model for $130V$ the values for one single battery cell of $3.7V$ can easily be derived:

Parameters for a single cell of $3.7V$			
R_{DC}	...	0.0303Ω	Seriel connection
L_{HF}	...	$6.277nH$	Seriel connection
C_{HF}	...	$364nF$	Parallel connection

To achieve the model for $300V$, 81 single cells have to be put in series.
For a DC-resistance of $400m\Omega$, 6 rows are connected in parallel, depicted in figure (7.4). Therefore the parameters for the final model are:

Parameters for: $300V$ and DC- resistance of $400m\Omega$		
$n = 81$ seriel connections, $k = 6$ parallel connections		
R_{DC}	$0.0303\Omega \cdot \frac{n}{k}$	$408m\Omega$
L_{HF}	$6.277nH \cdot \frac{n}{k}$	$84nH$
C_{HF}	$364nF \cdot \frac{k}{n}$	$29.6nF$

Calculation of the Parameter C_P

The approximate value for this parameter is obtained from the geometry of a battery cell.

$$\begin{aligned} C_{P_{cell}} &= \epsilon_0 \epsilon_r \frac{hln}{d} = 20pF \\ C_{P_{module}} &= \epsilon_0 \epsilon_r \frac{hl}{d} \frac{m}{n} = 8.64pF \end{aligned} \tag{7.1}$$

h	$0.15m$	height of the plate
l	$0.15m$	length of a plate
d	$0.001m$	distance between the plates
m	35	number of plate pairs per cell
k	81	number of cells connected in series
ϵ_r	110	permittivity, instancing acid sulfur

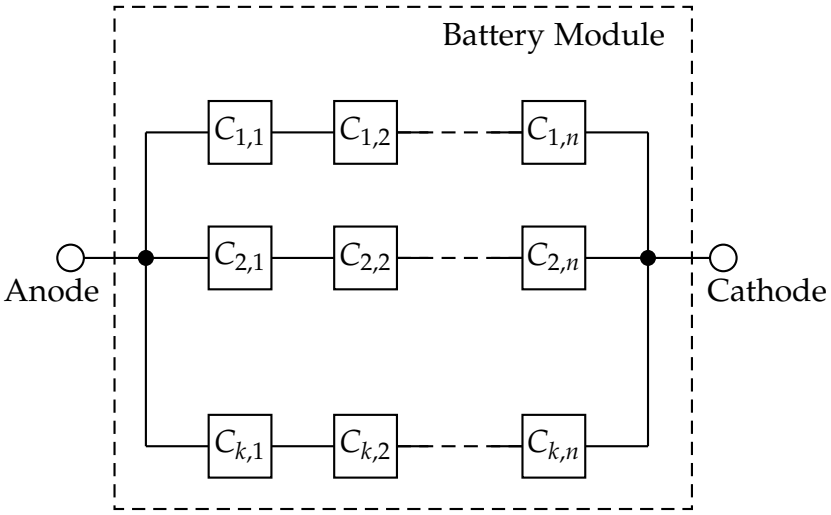

Figure 7.4: Battery Module

7.2 Line Impedance Stabilization Network

The Line Impedance Stabilization Network (LISN) is used for measurements of conducted emission. Its function is to provide a defined impedance and it also isolates the equipment, that has to be tested, from disturbances caused by the power supply.
The LISN used is a *Single path high voltage AMN (LISN) NNHV 8123-400* from SCHWARZBECK MESS- ELEKTRONIK and its circuit diagram is depicted in figure (7.5).

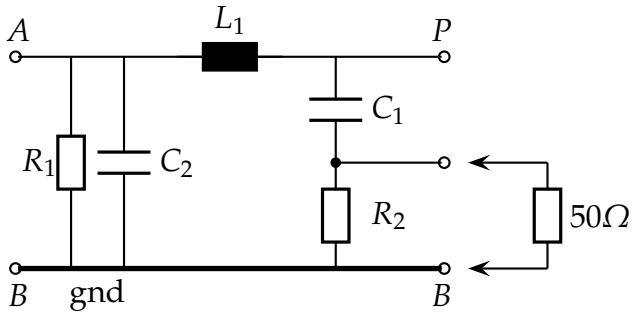

R_1 ... $1M\Omega$
C_2 ... $100nF$
L_1 ... $5\mu H$
C_1 ... $100nF$
R_2 ... $1k\Omega$

Figure 7.5: LISN

Impedance Mismatch

During component measurements, the disturbance sources should behave equally like they do in the real environment of the vehicle. The LISN therefore should model the wiring system as accurate as possible.
The input impedance of the LISN is 50Ω. Since the HV- cables, that are used, have a typical impedance of 6Ω to 20Ω, a mismatch at the connection to the LISN occurs. This causes reflections and therefore the measured levels can be biased.
In (**18**) a possibility for an impedance matching filter is proposed, see also figure (7.6). In figure (7.7) the input impedances of the LISN are illustrated with impedance transforming filter and without.
In this case the impedance is 10Ω since this is the nominal impedance of the cable used for this work.

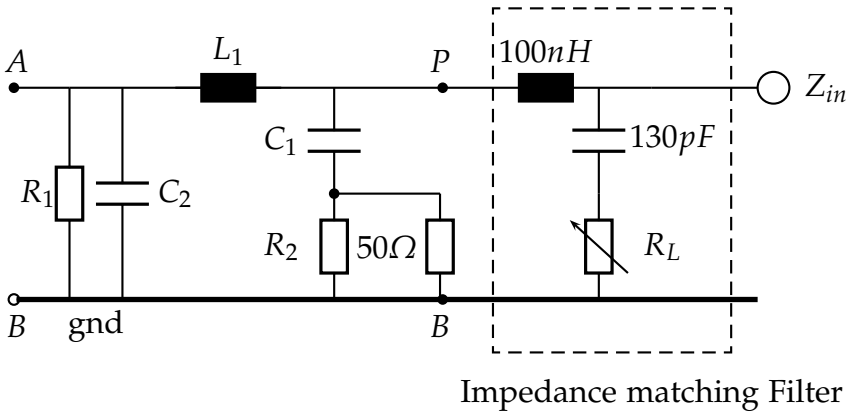

Figure 7.6: Filter for Impedance Matching

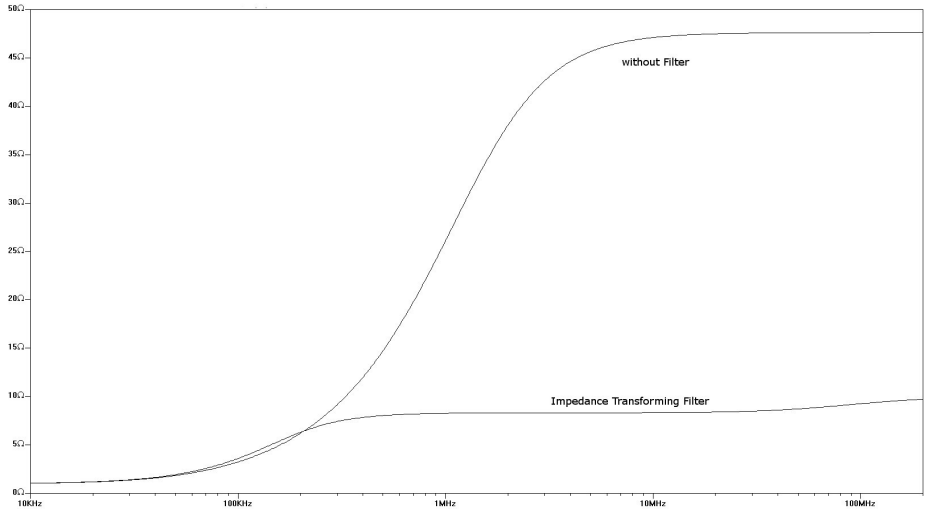

Figure 7.7: Input Impedance of the LISN

Figure (7.8) shows the cable input impedance according to the terminating impedance. For this simulation the terminating impedance is represented by the LISN with the filter, matching the 10Ω of the cable. The input impedance then is set to 10Ω and then to 50Ω.

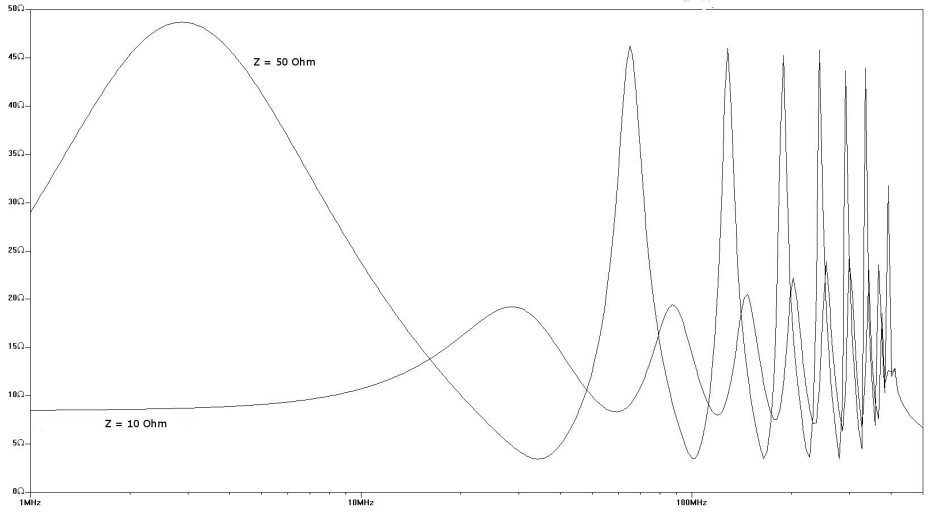

Figure 7.8

Even though the effect of mismatch is quite obvious, the impedance matching filter is not included in any standard.

Symmetrical Setup

For the simulation setup, two LISNs are symmetrically connected between the HV- battery and the HV- cables, as illustrated in figure (7.1). Via the measurement ports the conducted disturbances can be measured.
The circuit is shown in figure (7.9).

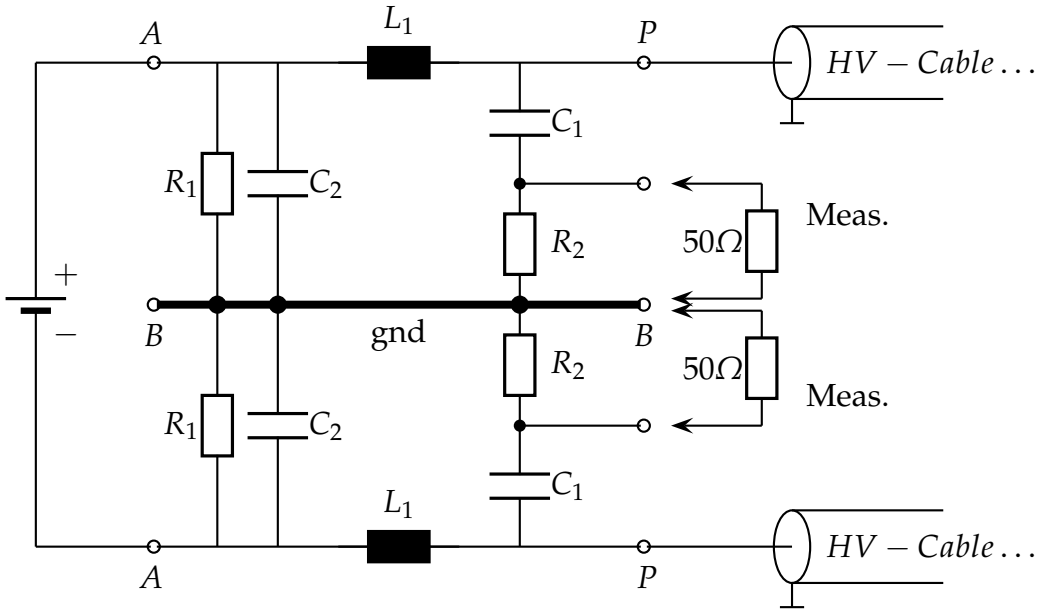

Figure 7.9: Symmetrically connected LISNs

7.3 HV- Cable

The cable used are again the HV- cables from COROPLAST, as described in chapter (4). The inductance calculation is for two parallel wires above a ground plane. The self inductances L_{ii} are calculated as in equation (3.28) and the mutual inductances are derived from equation (3.29).

The parameters are:

c	radius of the outer conductor	$6.8mm$
h	height of the cable above ground	$50mm$
s	distance between the two wires	$200mm$

$$\begin{aligned} L_{11} = L_{22} &= \frac{\mu_0}{2\pi} \ln\left(\frac{2h}{c}\right) \\ &= 537.7 \quad nH/m \\ L_{12} = L_{21} &= \frac{\mu_0}{2\pi} \ln\left(1 + \frac{4h^2}{s^2}\right) \\ &= 22.3 \quad nH/m \end{aligned}$$

The coupling factor between the two cables is:

$$k = \frac{L_{12}}{sqrtL_{11}L_{12}} = 0.2$$

The capacitance matrix is calculated as in equation (3.32).

$$\begin{aligned} C &= \mu_0\epsilon_0 L^{-1} \\ C &= \mu_0\epsilon_0 \begin{pmatrix} 537.7nH & 22.3nH \\ 22.3nH & 537.7nH \end{pmatrix}^{-1} \\ &= \begin{pmatrix} 20.73pF & -0.86pF \\ -0.86pF & 20.73pF \end{pmatrix} \end{aligned}$$

Therefore the capacitance values are:

$$\begin{aligned} C_{11} = C_{22} = &\quad 19.8pF/m \\ C_{12} = C_{21} = &\quad 0.86pF/m \end{aligned}$$

The schematics are like the ones in figure (6.1) and figure (6.2), except different parameters for L_{ii}, C_{ii}, C_{ij} and the coupling factor k.

7.4 Link Capacitance and Inverter

Link Capacitance

The link capacitance is used in the intermediate circuit of the converter. It couples electrical networks to one DC level. It also supports the DC voltage intermediate curcuit.
The equivalent circuit diagram is shown in figure (7.10).
The values are taken for the capacitance: *Kemet* $C4EEGMX6500AAUK$, *DC Link Capacitor for HybridPACK*^{TM}2.
The values for equivalent circuit are:

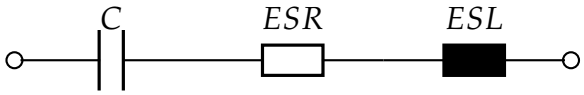

Figure 7.10: Link Capacitance

C	$500\mu F$
ESR	$1m\Omega$
ESL	$15nH$

Power Converter

Power converter are one of the main sources for interference.
The first cutoff- frequency results from the frequency of modulation and the second is caused by the switching frequency of the high speed switching devices. (IGBT, insulated gate bipolar transistor.)
The models for the IGBTs used for the simulation are for *IGBT* $1200V$ *TRENCHSTOP, Infineon*. The schematic of the inverter and the link capacitance can be seen in figure (7.11).

The parameters for the motor simulation are:

R_L	L_L
0.15Ω	$L_L = 300\mu H.$

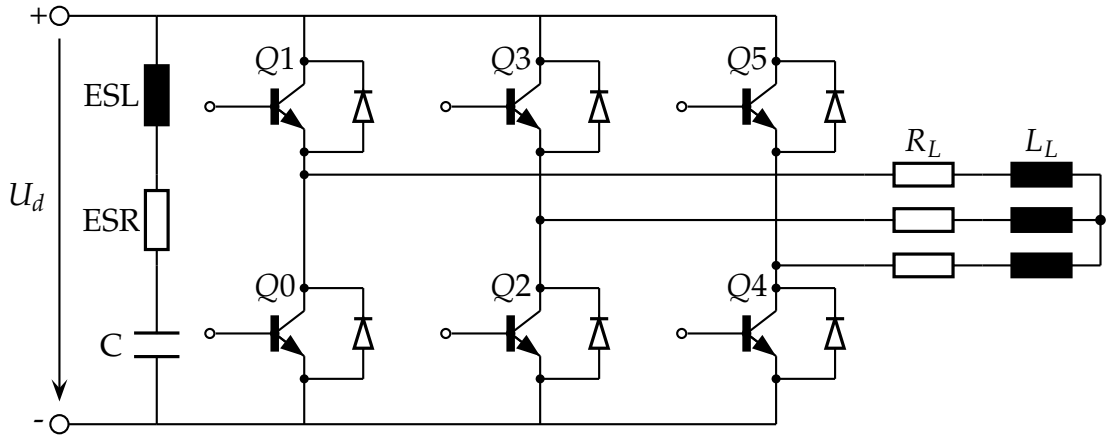

Figure 7.11

PWM-Control

The pulse width modulation control (pwm) signal has a duty cycle of 5% and its frequency is $20kHz$.
The control signals are phase-delayed by 120°. The signals for all three switches can be seen in figure (7.12). For the input Q_1 and the inverted input Q_0 they are depicted in figure (7.13)

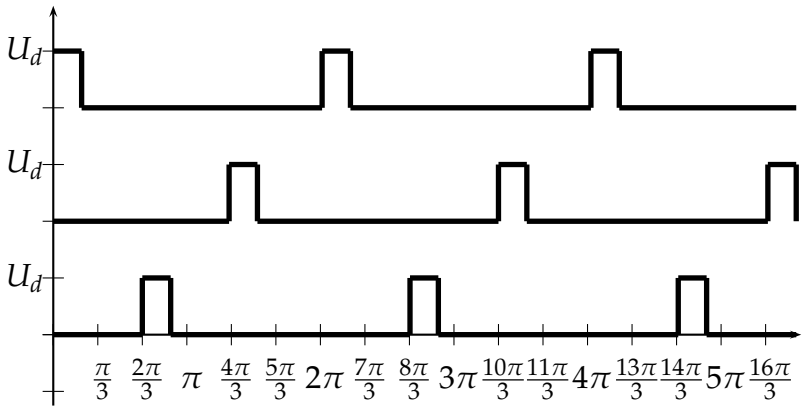

Figure 7.12: Control Signals

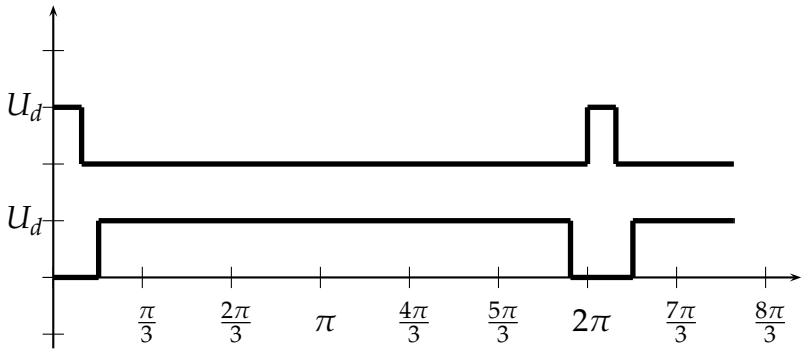

Figure 7.13: Signal and inverted Signal

7.5 Results

Simulation Setup 1

The disturbances on the HV- cables are simulated in this setup, as depicted in figure (7.1). The LISNs are symmetrically connected as shown in figure (7.9). One simulation was done with the filter for impedance matching, as in figure (7.6), and the results are printed in figure (7.14). On the contrary the results for the LISN without impedance matching can be seen in figure (7.15) and figure (7.16) .

The simulated results are:

Filter		Without Filter	
$V_{mess,peak-peak}$	$4.24V$	$V_{mess,peak-peak}$	$9V$
$I_{mess,peak-peak}$	$84.4mA$	$I_{mess,peak-peak}$	$160mA$

Although the results with the filter applied, are improved, it is has to be mentioned again, that till now, it is not part of any standard specification.

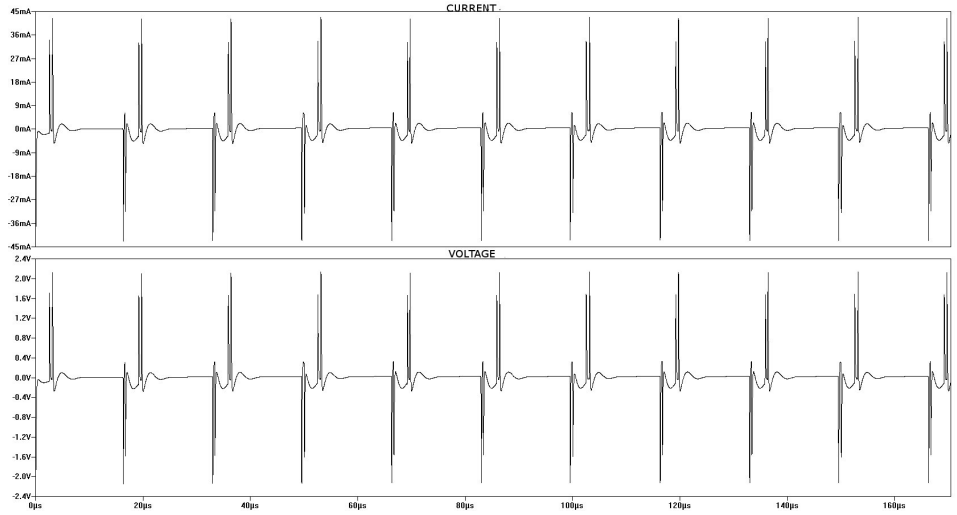

Figure 7.14: Simulation with Impedance Transforming Filter

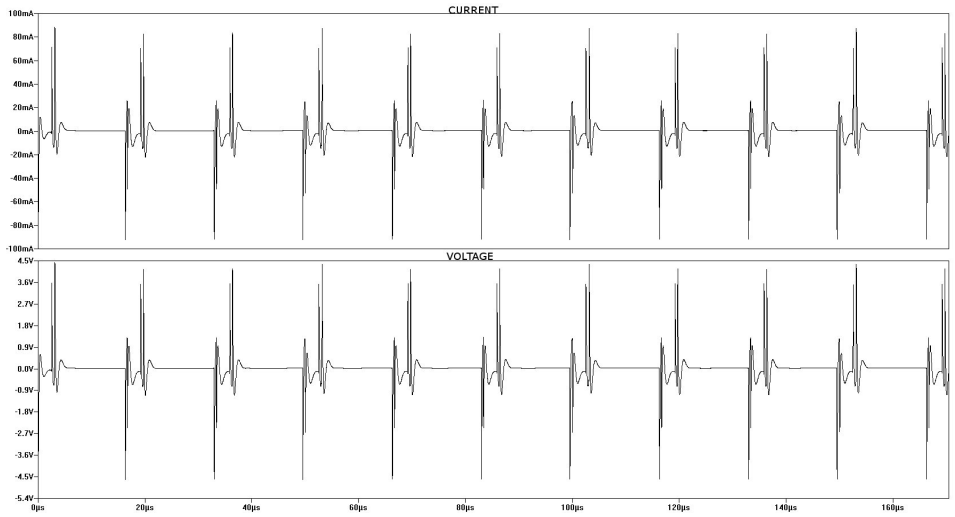

Figure 7.15: Simulation without Impedance Transforming Filter

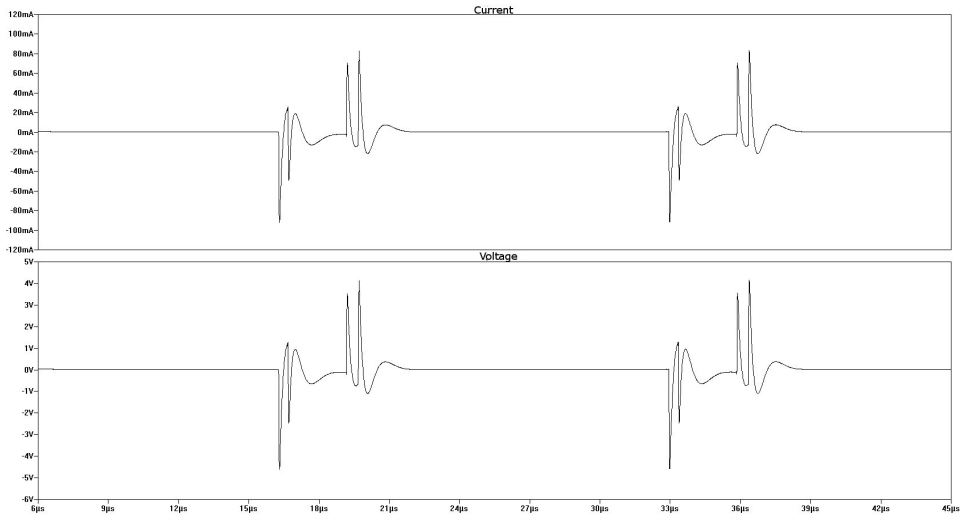

Figure 7.16

Simulation Setup 2

With this setup, as depicted in figure (7.2), the overall disturbances of the electric drive system should be measured.
There is no LISN for emulation of the line impedance used, since the idea is, to imitate real conditions.
Only the capacitance C_1 with $100nF$ and R_2 with 1000Ω from the LISN is used, figure (7.5).
The results can be seen in figures (7.17) and (7.18).

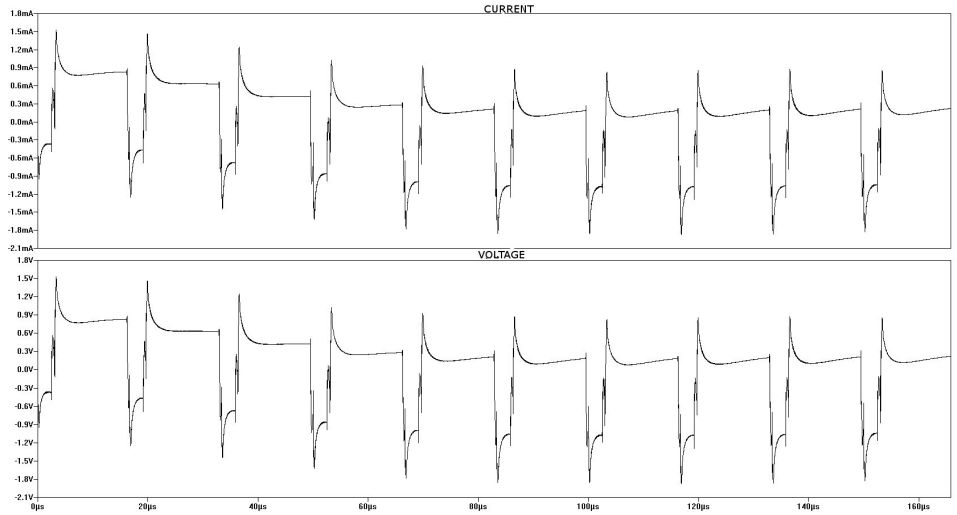

Figure 7.17

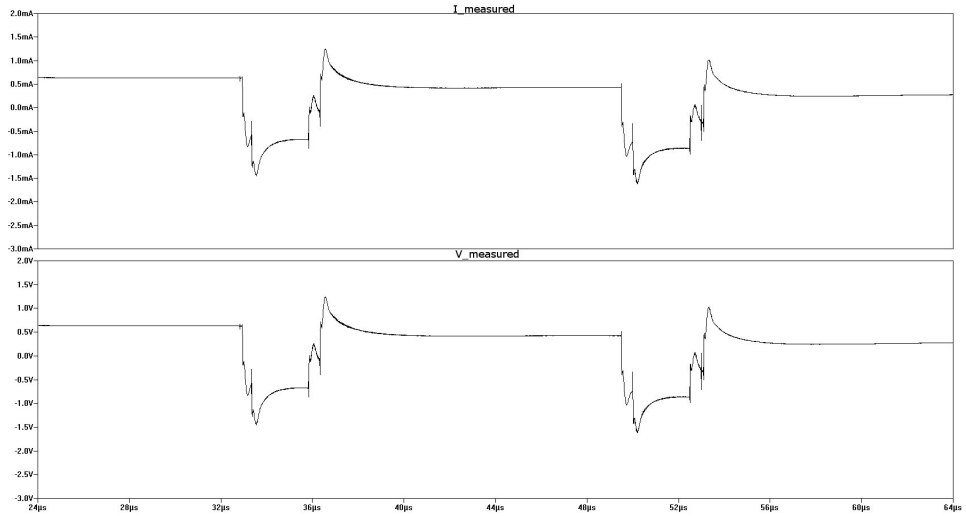
I_measured
2.0mA
1.5mA
1.0mA
0.5mA
0.0mA
-0.5mA
-1.0mA
-1.5mA
-2.0mA
-2.5mA
-3.0mA
V_measured
2.0V
1.5V
1.0V
0.5V
0.0V
-0.5V
-1.0V
-1.5V
-2.0V
-2.5V
-3.0V
24µs
28µs
32µs
36µs
40µs
44µs
48µs
52µs
56µs
60µs
64µs

Figure 7.18

8 Conclusion

The modeling of the cables, as described in section (4), gives a short overview, of how to gather schemes that are valid for high frequencies, with relatively little effort.
This models can be simulated quite easily with any generic circuit simulator. As an example, for this work , the simulation tool LTSpice was used.

The model derived for the capacitive coupling clamp can be used according to the *ISO 7637* and the $IEC61000-4-4$, as mentioned in section (5).

In chapter (7), important components for EMC- analysis of the electric drive system have been modeled.

In summary, deriving exact models that are suitable for EMC- analysis is very difficult. The geometry plays an important role, many assumptions have to be made and therefore the reality can never be represented exactly.

Nevertheless, using this kind of simulations as an supportive tool during development is justified, since they are helpful as an early evaluation method and assessment tool. Therefore they can support EMC-compliant design from the beginning.

Bibliography

[1] INTERNATIONAL STANDARD ISO 7637-2:2011, Third edition, *Road vehicles - Electrical disturbances from conduction and coupling - Part 2: Electrical transient conduction along supply lines only*

[2] IEC 61000-4-4 Edidion 3.0 2012-04, *Electromagnetic compatibility(EMC) - Part4-4: Testing and measurement techniques - Electrical fast transient/burst immunity test*

[3] Magdowski, M.; Vick, R., *Estimation of Mathematical Parameters of Double-Exponential Pulses Using the Nelder-Mead Algorithm*

[4] Clayton A. Paul, *Introduction to Electromagnetic Compatibility, 2nd Edition*

[5] Robert A. Chipman, *Theory and Problems of Transmission Lines*

[6] William H. Hayt, John A. Buck *Engeneering Electromagnetics*

[7] Clayton R. Paul, *Analysis of Multiconductor Transmission Lines, 2nd Edition*

[8] Bidyut K. Sen, Richard L. Wheeler, *Skin Effect Models for Transmission Line Structures using Generic SPICE Circuit Simulators*

[9] S. Kim, D.P. Neikirk, *Compact Equivalent Circuit Model for the Skin Effect*

[10] INTERNATIONAL STANDARD ISO 7637-3:2007, Second Edition, *Road vehicles - Electrical disturbances from conduction and coupling - Part 3: Electrical transient transmission by capacitive and inductive coupling via lines other then supply lines*

[11] Franceso Musolino, Franco Fiori, *Modeling the IEC 61000-4-4 EFT Injection Clamp*

[12] Edward G. Cristal, *Coupled Circular Cylindrical Rods Between Parallel Ground Planes*

[13] J.T. Bolljahn, G.L. Matthaei, *A Study on the Phase and Filter Properties of Arrays of Parallel Conductors Between Ground Planes*

[14] A.E. Ruehli, *Inductance Calculations in a complex Integrated Circuit Environment*

[15] Clayton R. Paul, *Inductance, Loop and Partial*

[16] Brian Young, *Return Path in Measurements of Package Inductance Matrices*

[17] VDA, Verband der Automobilindustrie, *Systemmodellierung für Komponenten von Hybridfahrzeugen unter Berücksichtigung von Funktions- und EMV Gesichtspunkten*

[18] Martin Reuter, Manuel Waible, Stefan Tenbohlen, Wolfgang Köhler, *Einfluss der Abschlussimpedanz von Hochvoltkabeln auf Funkstörgrössen in elektrisch angetriebenen Fahrzeugen*